Journal of Controlled Release 352 (2022) 422–437

Contents lists available at ScienceDirect

Journal of Controlled Release

journal homepage: www.elsevier.com/locate/jconrel

Airway epithelial cell-specific delivery of lipid nanoparticles loading siRNA for asthma treatment

Mengjun Zhang [a], Huiyang Jiang [a], Lan Wu [a], Haoyu Lu [a], Hriday Bera [a,b], Xing Zhao [a], Xiong Guo [a], Xulu Liu [a], Dongmei Cun [a,*], Mingshi Yang [a,c,*]

[a] Wuya College of Innovation, Shenyang Pharmaceutical University, Wenhua Road, No. 103, 110016 Shenyang, China
[b] Dr. B.C. Roy College of Pharmacy & Allied Health Sciences, Durgapur, West Bengal, 713212, India
[c] Department of Pharmacy, Faculty of Health and Medical Sciences, University of Copenhagen, Universitetsparken 2, DK-2100 Copenhagen, Denmark

ARTICLE INFO

Keywords:
Pulmonary delivery
siRNA
Lipid nanoparticles
Asthma
Airway epithelial cells

ABSTRACT

With specific and inherent mRNA cleaving activity, small interfering RNA (siRNA) has been deemed promising therapeutics to reduce the exacerbation rate of asthma by inhibiting the expression and release of proinflammatory cytokines from airway epithelial cells (AECs). To exert the therapeutic effects of siRNA drugs, nanoformulations with high efficiency and safety are required to deliver these nucleic acids to the target cells. Herein, we exploited novel inhaled lipid nanoparticles (LNPs) targeting intercellular adhesion molecule-1 (ICAM-1) receptors on the apical side of AECs. This delivery system is meant to enhance the specific delivery efficiency of siRNA in AECs to prevent the expression of proinflammatory cytokines in AECs and the concomitant symptoms in parallel. A cyclic peptide that resembles part of the capsid protein of rhinovirus and binds to ICAM-1 receptors was initially conjugated with cholesterol and subsequently assembled with ionizable cationic lipids to form the LNPs (Pep-LNPs) loaded with siRNA against thymic stromal lymphopoietin (TSLP siRNA). The obtained Pep-LNPs were subjected to thorough characterization and evaluations *in vitro* and *in vivo*. Pep-LNPs significantly enhanced cellular uptake and gene silencing efficiency in human epithelial cells expressing ICAM-1 *in vitro*, exhibited AEC-specific delivery and improved the gene silencing effect in ovalbumin-challenged asthmatic mice after pulmonary administration. More importantly, Pep-LNPs remarkably downregulated the expression of TSLP in AECs, effectively alleviated inflammatory cell infiltration, and reduced the secretion of other proinflammatory cytokines, including IL-4 and IL-13, as well as mucus production in asthmatic mice. This study demonstrates that Pep-LNPs are safe and efficient to deliver siRNA drugs to asthmatic AECs and could potentially alleviate allergic asthma by inhibiting the overexpression of proinflammatory cytokines in the airway.

1. Introduction

Asthma is one of the most common chronic inflammatory disease of the lung characterized by varied degrees of airway inflammation, airway obstruction, mucus hypersecretion, and airway hyperresponsiveness (AHR) [1]. Asthma affects >300 million people and causes death in approximately 0.4 million people annually worldwide [2,3]. Due to its complex pathophysiology and multifactorial etiology, asthma still remains incurable. Traditional treatment methods, such as use of bronchodilators and anti-inflammatory drugs, could provide only symptomatic relief but hardly prevent the progressive deterioration of lung function in asthmatic patients [1,4].

In recent years, studies on mechanisms of asthma have found that genetic risk factors can interact with inhaled environmental factors in multiple ways to contribute to asthma pathogenesis [5,6]. Increasing evidence suggests that many disease susceptibility genes are upregulated in asthmatic conditions [7,8]. Small interfering RNA (siRNA)-based therapeutics, as a new class of biologics following protein drugs, can specifically degrade target mRNA and have been used to suppress the expression of disease-relevant genes [9]. siRNA can be an attractive therapeutic alternative to small molecule drugs or monoclonal antibody drugs for the treatment of asthma due to its high specificity and

Abbreviations: AECs, Airway epithelial cells; LNPs, Lipid nanoparticles; ICAM-1, Intercellular adhesion molecule-1; TSLP, Thymic stromal lymphopoietin; AHR, Airway hyperresponsiveness; BALF, Bronchoalveolar lavage fluid.

* Corresponding authors at: Wuya College of Innovation, Shenyang Pharmaceutical University, Wenhua Road, No. 103, 110016 Shenyang, China.
E-mail addresses: cundongmei@163.com (D. Cun), mingshi.yang@sund.ku.dk (M. Yang).

https://doi.org/10.1016/j.jconrel.2022.10.020
Received 19 July 2022; Received in revised form 10 October 2022; Accepted 13 October 2022
Available online 31 October 2022

numerous promising targets [10,11].

TSLP is an upstream cytokine produced by airway epithelial cells (AECs) in response to pathogenic stimuli and plays a prominent role in triggering the inflammatory cascades by activating various immune cells [12]. Particularly, it can promote the proliferation and differentiation of T cells and stimulate the production of T helper (Th) 2 cytokines (such as IL-4 and IL-13), inducing goblet cell hyperplasia, bronchus hyperactivity and airway remodeling [12,13]. Studies have shown that multiple downstream inflammatory pathways can be inhibited by blocking TSLP [13,14]. Inhibiting the expression and release of TSLP from AECs at the gene level using siRNA drugs might be a promising strategy to alleviate airway inflammation and impede asthma progression.

Pulmonary delivery of therapeutics is the most straightforward method for the treatment of asthma and inhalation of siRNA has been reported as one of the most promising approaches for bringing siRNA targeting respiratory diseases to the clinic [15]. It can shorten the delivery path by directly applying the active substances close to the disease-related cells, reduce the dose required and prevent them from systemic nucleases and other complex components [16]. Despite several advantages of pulmonary administration, targeted siRNA delivery to the disease-relevant cells in the lung (*e.g.*, AECs) could be challenging. This is ascribed to the fact that the lung tissues are composed of a wide variety of cell types with variable functionalities and accessibility to siRNA therapeutics [16,17].

Studies have demonstrated that AECs express increased levels of surface markers and receptors associated with inflammatory cell infiltration and airway remodeling in asthmatic inflammatory conditions [18]. Among these surface markers, intercellular adhesion molecule-1 (ICAM-1), also known as CD54, is upregulated by inflammatory stimuli in asthma, and its expression level correlates with severity of the disease [19,20]. In fact, ICAM-1 plays an important role in cell adhesion and migration and serves as a principal receptor for the majority of rhinoviruses (RVs), which has been exploited as a target to design drug delivery vehicles for site-specific delivery of therapeutic agents into AECs [21–24]. Given that ICAM-1 is upregulated in asthma and located on the apical side of AECs, ICAM-1 is deemed an appealing receptor to be targeted to design a cell-specific siRNA delivery system *via* pulmonary administration.

Recent years have witnessed significant benefits of LNPs for nucleic acid therapeutics [25,26]. However, the delivery of siRNA using LNPs has been limited primarily by its poor delivery efficiency in extrahepatic tissues and cell types beyond hepatocytes [27]. In this current research endeavors, novel inhaled LNPs loaded with TSLP siRNA (siTSLP) were constructed to exert AEC-specific delivery of siRNA drugs to prevent the overexpression of TSLP and concomitant symptoms in parallel. To this end, a cyclic peptide (CSERSMNFC) ligand, which resembles part of the capsid protein of rhinovirus and efficiently binds to ICAM-1 receptors on the apical side of AECs, was chosen to modify LNPs to obtain the new LNPs (Pep-LNPs) [28]. We hypothesized that these siTSLP-loaded Pep-LNPs (Pep-LNPs-siTSLP) would enhance the AEC-specific delivery efficiency of the siRNA drugs *via* receptor-mediated endocytosis after pulmonary administration, inhibit the overexpression of TSLP and thus alleviate AHR and airway inflammation (Scheme 1). After thorough *in vitro* characterization and evaluation on the formulated LNPs including cellular uptake behavior and gene silencing efficiency in different lung cell lines, their cell population distribution, safety and gene silencing effects were systematically evaluated in mice after pulmonary administration. Last, the effects of Pep-LNPs-siTSLP on the expression of TSLP and other cytokines, inflammatory cell infiltration, mucus production and lung function were assessed in ovalbumin-challenged asthmatic mice.

2. Materials and methods

2.1. Materials

DLin-MC3-DMA (MC3), 1,2-dioleoyl-sn-glycero-3-phosphocholine dioleoyl phosphatidylcholine (DOPC), cholesterol and 1,2-dimyristoyl-

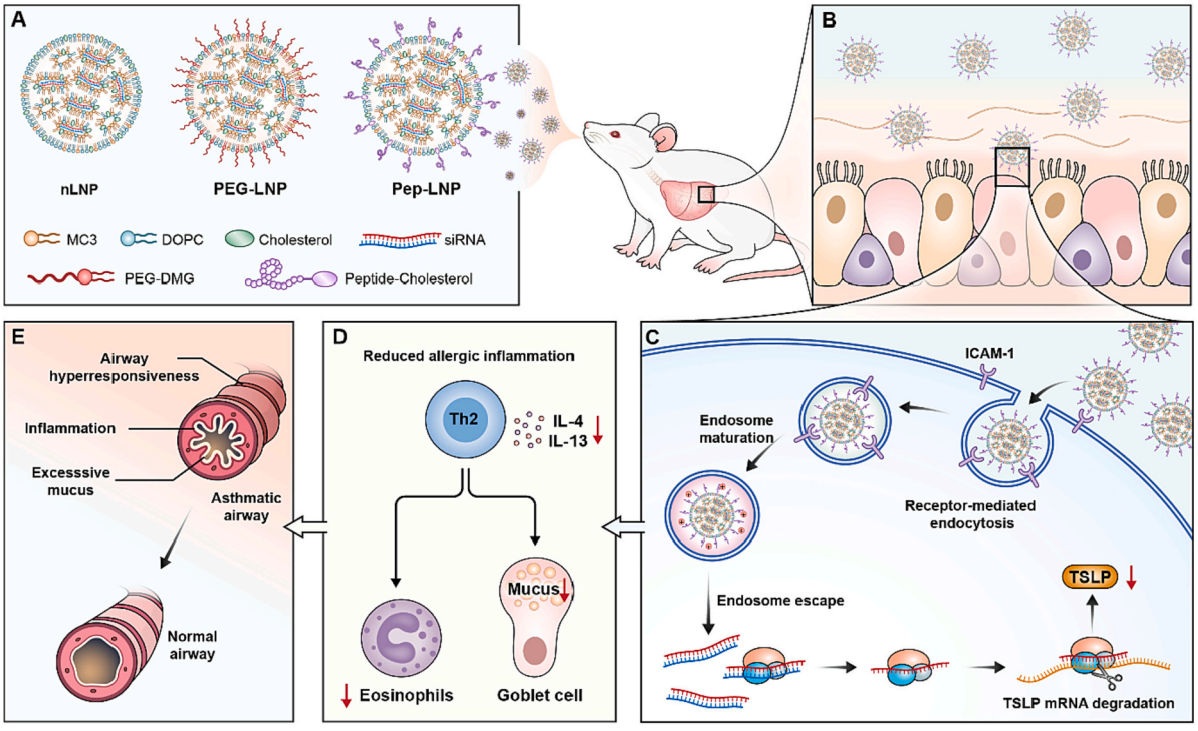

Scheme 1. Schematic illustration of AECs-specific delivery of LNPs-siTSLP alleviates allergic asthma *via* pulmonary administration. Different LNPs-siRNA exploited in this study (A); deposition of LNPs-siRNA in the airway post pulmonary administration (B); ICAM-1 receptor-mediated endocytosis of Pep-LNPs-siTSLP by AECs and the following RNA interfering action (C); suppression of the production of T helper (Th) 2 cytokines and the infiltration of eosinophils and over-secretion of mucin (D); alleviated airway inflammation in allergic asthma (E).

rac-glycero-3-methoxypolyethylene glycol-2000 (PEG-DMG) were purchased from AVT (Shanghai, China). The targeting peptide (NNGGGGCSERSMNFC) was synthesized and supplied by LifeTein Co., Ltd. (Beijing, China). Cholesteryl hemisuccinate (CHEMS), N-hydroxysuccinimide (NHS) and 1-(3-dimethylaminopropyl)-3-ethylcarbodiimide hydrochloride (EDC) were obtained from Aladdin (Shanghai, China). The Quant-iT™ RiboGreen® RNA Kit, Lipofectamine 2000, primary antibody against β-actin (clone 15GA11/E2) and HRP-conjugated secondary antibodies (goat anti-mouse IgG) were procured from Thermo Fisher Scientific (USA). A primary antibody against GAPDH (AC002) was purchased from ABclonal Technology Co., Ltd. (Wuhan, China). A primary antibody against MUC5AC (clone 45 M1) was purchased from Abcam (Shanghai, China). Mouse IL-6, IL-1β, TNF-α, IL-4, IL-13 and TSLP ELISA kits were supplied by NeoBioscience (Shenzhen, China). Mouse MUC5AC ELISA kit was purchased from JiangLai Biotech (Shanghai, China). GAPDH siRNA (siGAPDH), negative control siRNA (siNC) and fluorescently-labeled siRNA were provided by GenePharma (Shanghai, China). siRNA targeting TSLP (ON-TARGET-plus SMART pool® siRNA) was purchased from Dharmacon (USA). The sequences of the siRNA and primers used for RT–PCR are given in Table S1. All the other reagents utilized in this study were of analytical grade.

2.2. Cell lines and animals

The BEAS-2B epithelial cell line and A549 cell line were purchased from the Kunming Cell Bank, Chinese Academy of Sciences. 16HBE was received from Otwo Biotech Inc. (Shenzhen, China). Animal studies were carried out on female BALB/c mice (6–8 weeks) in accordance with the experimental protocols approved by the animal ethical committee, Shenyang Pharmaceutical University, China (No. SYPU-IACUE-C2021-11-18-105).

2.3. Synthesis and characterization of the peptide-cholesterol conjugate

The peptide-cholesterol conjugate (Pep-Chol) was synthesized according to the previously reported protocol with slight modifications [29]. Briefly, CHEMS (365.0 mg, 0.75 mmol), EDC (215.7 mg, 1.125 mmol) and NHS (129.5 mg, 1.125 mmol) were dissolved in dimethylformamide (DMF; 5 mL) and stirred at room temperature for 4 h. The peptide (1532.7 mg, 0.9 mmol) was then added to the solution and the reaction mixture was stirred at room temperature for another 48 h. The reaction mixture was then dialyzed (MW, 1500D) against deionized water for 48 h to remove the excess peptides and then lyophilized. The product was analyzed by ARX-300 spectrometer (BRUKER, Germany) to acquire its ^{1}H NMR spectra. The sample was also scanned under FTIR spectroscopy (Bruker IFS55, JASCO, Germany) over a wave number range of 4000–1000 cm^{-1}.

2.4. Preparation and characterization of the siRNA-loaded LNPs

siRNA loaded-LNPs (LNPs-siRNA) were prepared using the stepwise ethanol dilution method [27,30,31]. The lipid components, consisting of MC3 lipids, DOPC and cholesterol (at a molar ratio of 1:1:1), were dissolved in anhydrous ethanol with a total lipid concentration of 5 mM. siRNA (N/P ratio, 20) dissolved into pH 4.0 citrate buffer (10 mM) was titrated into the lipid solution under vigorous stirring and rapidly diluted with citrate buffer (pH 4.0) to reduce ethanol concentration from 50 % *v*/v to 20% v/v. The ultrafiltration was then performed (MWCO 50 kDa, Millipore) to remove ethanol and free siRNA and the external buffer of the LNPs-siRNA was replaced with PBS (pH 7.4) and then concentrated. A similar method was adopted to formulate PEG-LNPs-siRNA and Pep-LNPs-siRNA, except the addition of PEG-DMG and Pep-Chol, respectively to the above lipid solution at a certain molar ratio. The size distribution and zeta potential of these nanoparticles were measured with a Nano ZS Zetasizer instrument (Malvern, UK). The LNPs-siRNA were dropped onto a copper grid, stained with 2.0% phosphotungstic acid and air dried, and subsequently their morphological characteristics were observed by transmission electron microscopy (TEM; Hitachi, Tokyo, Japan).

2.5. Encapsulation efficiency and RNase stability of siRNA

To investigate the siRNA loading capability, the total siRNA and free siRNA in the LNP formulations were measured using a Quant-iT™ RiboGreen® RNA Kit by comparing fluorescence in the presence and absence of 0.1% Triton X-100, respectively [30]. The encapsulation efficiency (%) was calculated based on the following equation.

$$\text{Encapsulation efficiency (\%)} = \frac{\text{W total siRNA} - \text{W free siRNA}}{\text{W total siRNA}} \times 100\%$$

An agarose gel electrophoresis-based retardation assay was also used to evaluate siRNA encapsulation efficiency and the protective effect of the LNPs. Briefly, free siRNA and LNPs-siRNA treated with Triton X-100 or PBS were loaded onto a 2% agarose gel containing Gel Red (Beyotime Biotechnology, China) and electrophoresed at 100 V for 30 min in Tris-acetate-EDTA (TBE) buffer. To evaluate the protection effect of the nanocarrier from nucleases, free siRNA or LNPs-siRNA were incubated with RNase A (0.1 mg/mL; Beyotime Biotechnology, China) or PBS at 37 °C for 30 min. Then, the samples were supplemented with ethylenediaminetetraacetic acid (EDTA, 1.5 mM) and incubated at 65 °C for 10 min to inactivate the enzymes [32]. These samples were treated with Triton X-100 before being assessed by agarose gel electrophoresis.

2.6. Cellular uptake

The *in vitro* cellular uptake efficiency of Cy3-siRNA-loaded LNPs was investigated using flow cytometry. Briefly, cells (A549, BEAS-2B or 16HBE) were seeded into 6-well plates (3×10^5 cells/well). After incubated overnight, cells were treated with Cy3-siRNA-loaded LNPs in DMEM medium (Dulbecco's modified eagle medium, Dalian Meilun Biotechnology, China) at an equivalent concentration of siRNA (50 nM), incubated at 37 °C for 6 h. The cells were washed three times with ice-cold PBS, harvested and resuspended in 0.5 mL of PBS and subjected to flow cytometry (BD FACSCalibur, USA).

2.7. Intracellular location of LNPs-siRNA by confocal laser scanning microscopy

The intracellular distribution of Cy3-siRNA-loaded LNPs was investigated by confocal laser scanning microscopy (CLSM). Cells at a density of 2×10^5 were seeded on glass-bottomed dishes (diameter, 20 mm) and incubated overnight. Cy3-siRNA-loaded LNPs were diluted in DMEM medium and incubated with the cells for 6 h at 37 °C. After that, the cells were washed with PBS three times and stained with 1 mL of LysoTracker (Beyotime Biotechnology Co., Ltd., Shanghai, China; 1:2500 dilution) for 30 min at 37 °C. After rinsing with PBS three times, the cells were fixed with 4% paraformaldehyde. The nuclei were marked with 4′,6-diamidino-2-phenylindole (DAPI; Dalian Meilun Biotechnology, China) and then visualized by CLSM (Olympus FV1000-IX81, Japan). Pearson's coefficient was determined by Image pro Plus 6.0.

2.8. In vitro gene silencing effect

2.8.1. Real-time PCR (RT-PCR)

To evaluate the transfection efficiency of the delivery systems in three different cell lines, GAPDH siRNA (siGAPDH) was used as a model siRNA. Cells were seeded in 12-well plates (6×10^4 cells/well) and cultured for 24 h. The cells were treated with LNPs loaded with siGAPDH or negative control siRNA (siNC) (50 nM) in DMEM medium and cultured for another 48 h. PBS and Lipofectamine 2000 (Lipo2000) were used as the blank and positive control, respectively. Total RNA was extracted from the cells using TRIzol reagent according to the

manufacturer's instructions. cDNA synthesis was performed using the PrimeScriptTM RT Reagent Kit (Takara, Japan). Real-time PCR amplification and evaluation were performed with TB Green Premix Ex Taq II (Takara, Japan) using a Stratagene Mx3005P (Agilent Technologies). Cycle threshold (Ct) values were determined by MxPro software (Agilent Technologies). The housekeeping gene β-actin was chosen as an internal control to normalize the GAPDH gene. The mRNA level of the target gene was calculated using the ΔΔCt method [33].

2.8.2. Western blot assay

Western blot assay was also used to evaluate the gene silencing effect of different LNP formulations. Cells were seeded in 6-well plates (2×10^5 cells/well) in DMEM medium and cultured for 24 h. The cells were treated with LNPs loaded with siGAPDH or siNC (50 nM) and then cultured for another 48 h. These cells were collected and lysed in RIPA lysis buffer containing 1% phenylmethanesulfonyl fluoride (PMSF). The protein contents in the cell lysates were quantified using a BCA kit and then boiled with protein loading buffer. Subsequently, the protein samples were fractionated by 10% SDS–PAGE, transferred to PVDF membranes and incubated with primary antibodies (1: 2000 dilution) at 4 °C overnight. After washing with TBST, the membranes were incubated with the corresponding HRP-conjugated secondary antibodies (1, 5000 dilution) at 25 °C for 1 h and washed again with TBST. The designated proteins were detected using ECL substrate by a Gel Imager System (Bio-Rad, USA). The protein β-actin was used as an internal standard.

2.9. In vivo lung accumulation and biodistribution

Female BALB/c mice were anesthetized with intraperitoneal (*i.p.*) injection of 5% choral hydrate and Cy5-siRNA-loaded LNPs or free Cy5-siRNA (25 μL, 4 μg of siRNA/mouse) were administered using intratracheal microspray (HRH-MAG4, Yuyan Instruments Co. Ltd., China). Then, the lungs and other vital organs were excised, washed with saline, and radiant efficiency intensity (ROI) of the lung tissue were measured with an IVIS Spectrum imaging system (PerkinElmer, USA).

2.10. Airway distribution and cellular localization

Cy3-siRNA-loaded LNPs (25 μL, 4 μg of siRNA/mouse) were administered to the anesthetized BALB/c mice *via* intratracheal microspray. The lungs of the treated mice were harvested at 0.5 h or 4 h post-administration, fixed with 4% paraformaldehyde overnight and flash-frozen in Optimal Cutting Temperature (OCT) compound (Fisher Healthcare). Cryosections of the lung tissue (10 μm) were obtained and stained with DAPI. Images of the cryosections were captured by CLSM (Olympus FV1000-IX81, Japan).

2.11. Animal model of OVA-challenged asthma

The OVA-challenged asthma model was established based on the method reported previously [34]. Briefly, BALB/c mice (female, 18–20 g) were sensitized by intraperitoneal (*i.p.*) injection of a 0.2 mL suspension of ovalbumin (OVA) and $Al(OH)_3$ (0.5 mg/mL of OVA, and 0.75 mg/mL of $Al(OH)_3$ in PBS (pH 7.4)) on Day 0 and 7. The sensitized mice were then exposed to aerosolized 2% (*w/v*) OVA solution in PBS (pH 7.4) produced by a compressed air atomizer for 30 min on Day 14–42. Mice sensitized and aerosolized with PBS (pH 7.4) were used as the normal control group.

2.12. Distribution of LNPs-siRNA in various lung cell populations

To test the distribution of LNPs-siRNA in different lung cell types, lungs from both healthy and asthmatic mice were obtained 8 h after pulmonary administration of Cy5-siRNAloaded LNPs (25 μL, 4 μg of siRNA/mouse). To prepare the lung single-cell suspensions, the isolated lungs were minced and digested using FBS-free DMEM containing 1 mg/mL collagenase D (Roche) and 0.1 mg/mL DNase I (Roche) at 37 °C for 30 min with shaking. The acquired cell suspension was then strained through a 40 μm cell strainer (JET BIOFIL, China). Red blood cells (RBCs) in the cell suspensions were lysed using 1 × RBC Lysis Buffer (Meilun Biotechnology Co., Ltd., Dalian, China) and then washed twice with PBS. The cell pellets were resuspended in 100 μL of PBS and then incubated with Fc Block (BD, USA) at 4 °C for 10 min, and the fluorochrome-conjugated antibodies (CD45-FITC (BD, 553079), CD31-PerCP-Cy5.5 (BioLegend, 102522), CD326 (Ep-CAM)-PE-Cy7 (BioLegend,118216) and CD54 (ICAM-1)-PE (BD, 553253)) were added for incubation at 4 °C for 30 min [27,35]. The dose of each antibody were decided based on the manufacturer's instructions. The samples were analyzed using a multicolor flow cytometer (BD FACSAria™ III, USA). The gating scheme is illustrated in Fig. S2, and data analyses were analyzed using FlowJo software (BD, USA).

2.13. The therapeutic effects of Pep-LNPs against allergic asthma

2.13.1. Treatment with Pep-LNPs-siTSLP in asthmatic mice

The OVA-challenged asthmatic mice were dosed separately with PBS, Pep-LNPs-siTSLP and Pep-LNPs-siNC (25 μL, 4 μg of siRNA/mouse) at every three days (on Day35, 38 and 41) by intratracheal microspray for total three times (Fig. 6A). Forty-eight hours after the last administration (*i.e.*, 24 h after the last challenge with OVA or PBS), the lungs were harvested, and various biological samples were collected and analyzed as described below.

2.13.2. Measurement of AHR

Forty-eight hours after the last dose, animals were placed in the plethysmography chambers of a whole-body plethysmograph (WBP-4MR, TOW, China) [36]. After 20 min of acclimation in the cavity, the mice were nebulized with increasing concentrations of methacholine (Mch) (0, 3.125, 6.25, 12.5, 25, 50 and 100 mg/mL) through the atomization port of the chamber. The atomization process for each dose of Mch lasted 90 s, and the responses of the mice were recorded for 5 min and returned to baseline levels before the next atomization [37,38]. The enhanced pause (Penh) values were determined by ResMass 1.4.2 software (TOW, Shanghai, China.)

2.13.3. Analysis of immune cells and inflammatory cytokines

The levels of cytokines (TSLP, IL-4, IL-13) and respiratory mucin (MUC5AC) in the supernatants of BALF were quantified by ELISA kits according to the manufacturer's instructions. The cells collected from BALF were resuspended in 0.5 mL of PBS for cell counting. The cells were also spotted on glass slides and stained with Diff-Quick stain (Solarbio, Beijing, China). Eosinophils, lymphocytes and macrophages were counted according to their morphological appearances with a total of 200 cells per slide.

2.13.4. Lung histology and MUC5AC expression

For further histological analyses, the left lungs were collected and fixed with 4% paraformaldehyde for 24 h. Subsequently, paraffin sections of the lung tissue (5 μm) were obtained and hematoxylin-eosin (H&E) staining and periodic acid-schiff (PAS) staining were performed to evaluate lung inflammation and mucin production, respectively. The right lungs were homogenized in RIPA lysis buffer using a tissue homogenizer (Biosafer, Beijing, China) to acquire tissue protein products, and the MUC5AC expression level in the specimens was further determined by Western blotting.

2.14. Safety profiles

To access the safety profiles of the delivery system, BALB/c mice were intratracheally administered with LNPs-siRNA (siNC) (25 μL, 4 μg of siRNA/mouse) every three days for three times. Mice were also

treated with PBS and lipopolysaccharide (LPS) solution (2 μg/μL, 25 μL), which were used as the negative control and positive control, respectively. Twenty-four hours after the treatment, the mice were anesthetized, and the lungs were lavaged three times with 1 mL of PBS to collect lung bronchoalveolar lavage fluid (BALF). The BALF was centrifuged (1000 rpm, 10 min, 4 °C) and collect the supernatant to assay the concentrations of proinflammatory cytokine (IL-6, IL-1β and TNF-α) by ELISA techniques. The cells collected from the BALF were resuspended in PBS (pH 7.4, 0.5 mL) for total cell counting. Cells were spotted on glass slides and stained with Wright-Giemsa dye (Dalian Meilun Biotechnology, China). Macrophages and neutrophils were counted according to their morphology with a total of 200 cells per slide. The left lungs were fixed in 4% paraformaldehyde and stained with H&E to evaluate lung inflammation.

2.15. Statistical analysis

The data were analyzed by one-way ANOVA followed by Tukey's post-hoc test *via* SPSS software 16.0. A p-value <0.05 was considered statistically significant.

3. Results and discussion

3.1. Synthesis and characterization of the peptide ligand-modified cholesterol

AECs play an important role in airway inflammation and many asthma-associated proinflammatory cytokines, including TSLP, are overexpressed in AECs [8,18,39]. To achieve an efficient delivery of LNPs-sRNA to AECs, a cyclic peptide (CSERSMNFC) ligand was selected

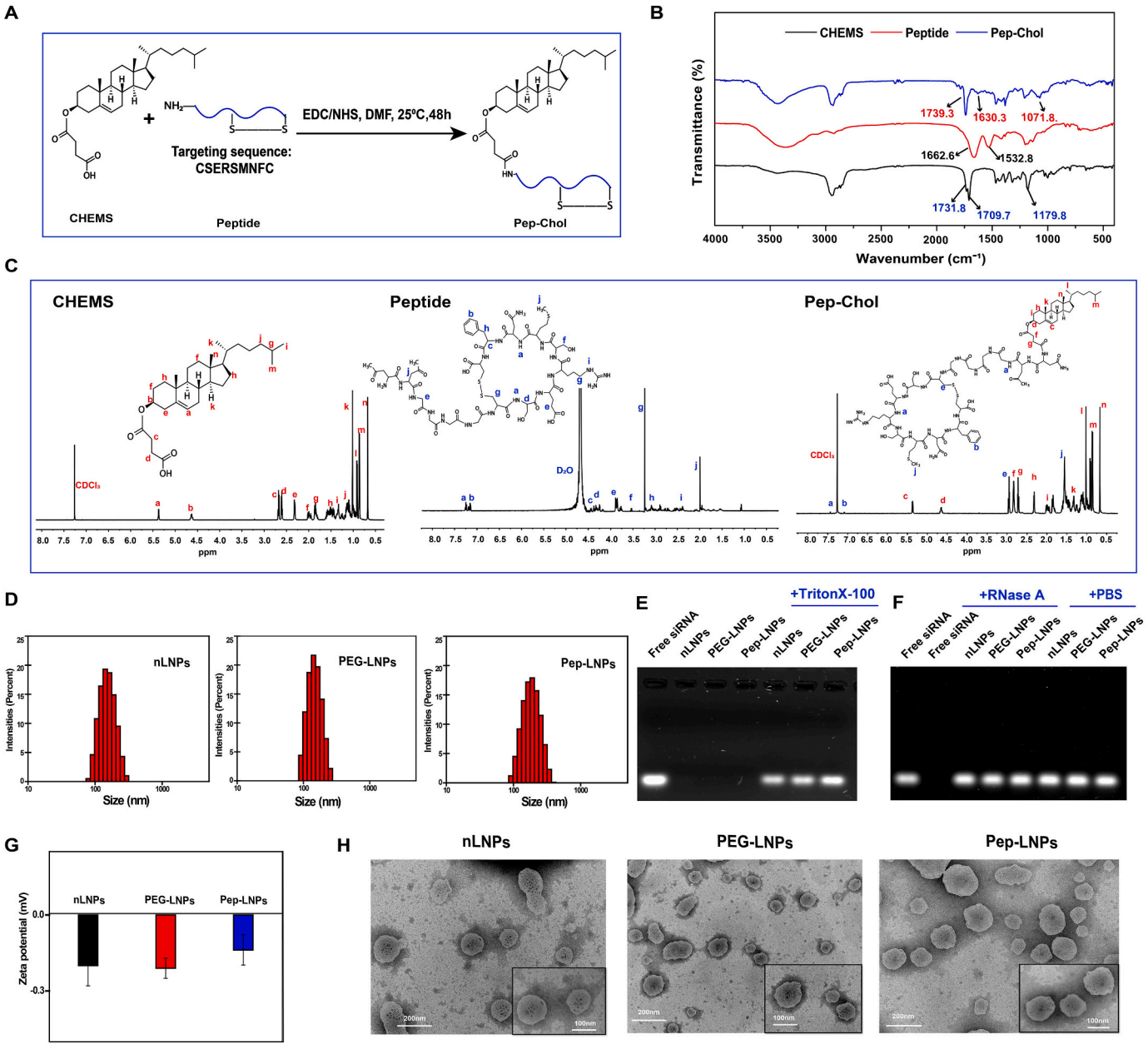

Fig. 1. Characterization of Pep-Chol and LNPs-siRNA. A schematic diagram of the synthesis of Pep-Chol (A). FT-IR (B) and ^{1}H NMR spectra (C) of CHEMS, peptide (NNGGGG-CSERSMNFC) and Pep-Chol. Particle size distributions (D) and zeta potential values (G) of the different LNPs (PEG-LNPs containing 1.6% PEG, Pep-LNPs containing 6.6% peptide) determined by DLS analyses. Agarose gel electrophoresis of LNPs-siRNA after the treatment with or without Triton X-100 (E). Protection ability of LNPs from siRNA degradation by RNase A (F). TEM images of the different formulations of LNP-siRNA (H).

to decorate the surfaces of the LNPs. This peptide screened through phage display technology displayed high affinity to the ICAM-1 receptor on the surface of AECs [28]. This unique characteristics of the cyclic peptide ligand could be attributed to the fact that its structure resembles part of the capsid protein of rhinoviruses [23]. In addition, the disulfide bridge between the two cysteines of the peptide ligand (Fig. 1A) could reduce the conformational freedom of the backbone, leading to its high stability and receptor selectivity [40,41].

To attach the peptide ligand to the surface of the siRNA-loaded LNPs, a short peptide (NNGGGG) was exploited as a linker to connect the peptide ligand (CSERSMNFC) and cholesterol molecules prior to their assembly with ionizable cationic lipids into LNPs. The linker peptide sequence was first attached to the cyclic peptide to obtain a new peptide, *i.e.*, NNGGGG-CSERSMNFC. This new peptide was subsequently conjugated with cholesteryl hemisuccinate (CHEMS) *via* an amide bond (Fig. 1A). As shown in the FT-IR spectrum (Fig. 1B), after the conjugation, the signals of CHEMS at 1709.7 cm^{-1} (C=O) and 1179.8 cm^{-1} (-C-O- stretching) were red shifted to 1630.3 cm^{-1} and 1071.8 cm^{-1}, respectively. These drifts could be attributed to the disappearance of the carboxylic acid groups of CHEMS and the formation of new amide bonds connecting the peptide and CHEMS [42].

The structure of the peptide-cholesterol conjugates (Pep-Chol) was also validated by ^{1}H NMR spectrum (Fig. 1C). The characteristic signals of the peptide moieties were resonated at δ 1.53 ppm (-SC$\underline{H}_3$), δ 2.92 ppm (-C$\underline{H}_2$-SCH$_3$), δ 7.45 ppm (-CO-N$\underline{H}$-) and δ 7.07 ppm (aromatic ring) in the spectrum of the conjugates. On the other hand, the cholesterol backbone in the conjugates could be confirmed by the typical peaks of alkyl chain protons appeared within δ1.02, 0.84 and 0.67 ppm. These results suggested that the Pep-Chol conjugates were successfully synthesized.

3.2. Preparation and characterization of LNPs-siRNA

LNPs-siRNA composed of the ionizable lipid MC3, cholesterol, and the neutral lipid (DOPC) was prepared by the ethanol dilution method, *i.e.*, nLNPs [27,30]. The peptide ligand-decorated LNPs (Pep-LNPs) and PEGylated LNPs (PEG-LNPs) were also formulated adopting similar methodology, but Pep-Chol and dimyristoyl glycerol (DMG)-polyethylene glycol (PEG) 2000 (PEG-DMG) were included to replace part of the cholesterol contents in the nLNPs. Previous studies have shown that PEG-lipids can improve the colloidal stability of LNPs [26]. Herein, both nLNPs and PEG-LNPs were used to compare the delivery efficiency of Pep-LNPs *via* pulmonary administration and better comprehend the function of the peptide ligand attached to the LNPs.

The hydrodynamic sizes of the nLNPs and PEG-LNPs were approximately 150 nm with a narrow size distribution (PDI < 0.2) (Table S1 and Fig. 1D). The incorporation of Pep-Chol in Pep-LNPs resulted in an increase in the particle size (180–190 nm). The zeta potential values of these LNPs were approximately 0.0–0.3 mV (Fig. 1G, Table S1). The surface charges of the nLNPs and PEG-LNPs are expected to be neutral, as the lipids used to prepare these formulations are neutral under physiological conditions [26]. The near neutral surface charge of the Pep-LNPs could be due to the isoelectric point of the peptide ligand, which is approximately 7.0. Therefore, the net charge of the peptide is close to neutral under physiological conditions [41]. The shapes of these LNPs were nearly spherical in shape as observed in the TEM images with the sizes ranging between 100 and 200 nm (Fig. 1H). The results of the colloidal stabilities studies conferred no significant changes in particle size of these LNPs during the storage at 4 °C for 14 days (Fig. S1), indicating their favorable storage stability.

The LNPs exhibited high encapsulation efficiency of siRNA (~90%) as determined by the RiboGreen® RNA assay (Table S1). The agarose gel electrophoresis assay displayed siRNA bands only after the LNPs-siRNA were treated with Triton X-100 (Fig. 1E). This result suggests that the siRNA was strongly associated with the lipids and encapsulated within the LNPs. The enzymatic stability of the siRNA in the LNP formulations was further investigated *via* agarose gel electrophoresis by incubating the these LNPs with RNase A or PBS. The results showed that LNPs protected the loaded siRNA from RNase A degradation. In contrast, free naked siRNA was completely degraded by RNase A (Fig. 1F).

In order to evaluate the structural stability of LNPs in BALF, fluorescence resonance energy transfer (FRET) technique was used to investigate the integrity of LNPs-siRNA during the incubation in the BALF. As shown in Fig. S2A, in the absence of the encapsulation of LNPs, the highly charged siRNAs remained far from one another in solution due to electrostatic repulsion. However, after encapsulated by LNPs, FRET signals were detected due to the short distance between of Cy5-siRNA and Cy3-siRNA [43]. The disassembly of LNPs and leakage of siRNA could result in the loss of FRET. The FRET signal was represented by the relative emission intensity of acceptor and donor and used to indicate structure integrity of the LNPs (Fig. S2B) [44]. The initial ratio of FRET was about 0.8 for all the three LNP formulations, which was still present at similar level after incubation for 8 h, indicating that these LNPs could remain intact in the BALF within 8 h. While, after incubation for 12 h, the FRET signal of nLNPs reduced to 0.68, suggesting that a proportion of siRNA might leak from nLNPs. nLNP without modification of hydrophilic molecules on the surface may undergo an increase in the amount of adsorbed proteins in the BALF, which could lead to the structural instability of the LNPs [45].

3.3. Pep-LNPs exhibit enhanced siRNA delivery efficiency in ICAM-1-expressing cells

Efficient cellular uptake of the LNPs is essential for successful siRNA transfection. To investigate the capability of the peptide ligand to improve the cellular uptake of the LNPs, three different cell lines, *i.e.*, 16HBE, BEAS-2B and A549, were exploited in this study. 16HBE and BEAS-2B cells are normal human bronchial epithelial cell lines expressing ICAM-1 [46–48]. A549 cells are adenocarcinomic human alveolar basal epithelial cells [49]. The cellular uptake efficiency of the Cy3-siRNA-loaded LNPs was evaluated by measuring the fluorescence intensity of the transfected cells using flow cytometry.

As shown in Fig. 2, the fluorescence intensities increased with raising the content ratios (*i.e.*, 1.6 % to 6.6 %, mol %) of the peptide ligand in the formulations in both 16HBE and BEAS-2B cells (Fig. 2A, B, D and E), which implied that the peptide ligand could enhance the cellular uptake of LNPs. Among different cell lines, BEAS-2B cells showed strongest cellular uptake of Pep-LNPs (Fig. 2D and E), which could be attributed to highest expression level of ICAM-1 on these cells compared with 16HBE and A549 cell lines (Fig. 2C, F, I and Fig. S3D). The lower ICAM-1 expression level on A549 cells might account for the limited effect of peptide ligand in improving cellular uptake (Fig. 2G, H and I). These results indicated the peptide ligand modification facilitated the cellular uptakes of siRNA-loaded Pep-LNPs effectively in cells with high expression level of ICAM-1.

The delivery efficiency of Pep-LNP with different peptide ratios was further verified by their gene silence effect based on RT-PCR (Fig. S3). The gene silencing efficiency of Pep-LNPs in both 16HBE cells (Fig. S3A) and BEAS-2B cells (Fig. S3B) were improved with increasing the proportion of the peptide ligand in the LNPs, which was consistent with the cellular uptake results. The Pep-LNPs consisting of 6.6% peptide ligand (6.6%-Pep-LNPs), which exhibited the highest gene silencing effect were chosen in the following studies for further investigation.

Additionally, our data confirmed that the siRNA delivery efficiency of PEG-LNPs were decreased with an increase in the PEG-DMG contents in the LNPs (Fig. S4), which was consistent with the previous studies [50,51]. As a higher level of PEGylation might hinder the siRNA delivery efficiency of LNPs, PEG-LNPs consisting 1.6% PEG-DMG were employed in the following studies.

To further confirm the RNAi effect of the Pep-LNPs after cellular uptake, the gene silencing efficiency was assessed at both the mRNA and protein levels using a model siRNA targeting GAPDH (siGAPDH) based

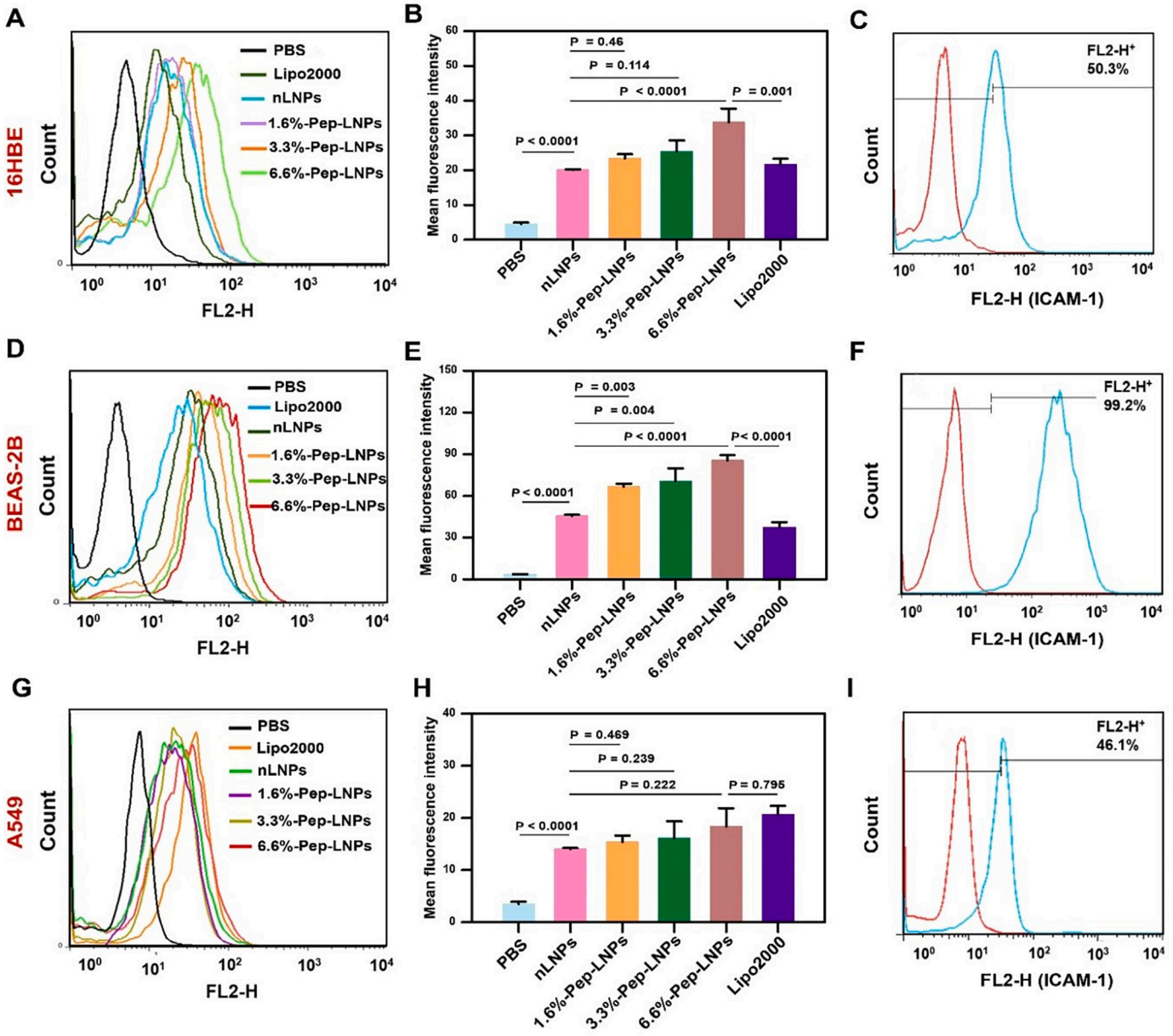

Fig. 2. Delivery efficiency of Cy3-siRNA-loaded LNPs with different proportions of peptide ligands. Cellular uptake efficiency measured by flow cytometry (A, B and C) and their mean fluorescence intensity (B, E and H) in three different cell lines. ICAM-1 expression level in different cell lines detected by flow cytometry: red curves represent untreated cells, blue curve represent cells treated with PE-labeled ICAM-1 antibody (C, F and I). Data are shown as the mean ± standard deviation (SD) (n = 3). (For interpretation of the references to colour in this figure legend, the reader is referred to the web version of this article.)

on RT-PCR and Western blot [52–54]. The Pep-LNPs exhibited more efficient gene silencing effect than the other two LNP formulations (*i.e.*, nLNPs and PEG-LNPs) in both 16HBE and BEAS-2B cells, and even better than that of Lipo2000 (Fig. 3A, B, D and E). Furthermore, among the three cell lines, Pep-LNPs displayed the highest gene silencing efficiency in BEAS-2B cells (Fig. 3B and E). These results suggest that the gene silencing efficiency of Pep-LNPs are cell line-dependent, which might be due to discrepancies in the expression levels of the ICAM-1 receptors on the cells and different intracellular trafficking mechanisms [54].

To investigate the subcellular location of these LNPs, endosomes were labeled with LysoTracker Green, and the intracellular colocalization of Cy3-siRNA-loaded LNPs and lysosomes were observed using CLSM and Pearson's coefficient was measured to evaluate the extent of correlation between signals of Cy3-siRNA and lysosome. In both 16HBE and BEAS-2B cells (Fig. 3G and H), the fluorescence signals of nLNPs and Pep-LNPs overlapped with LysoTracker Green to a lesser extent compared to PEG-LNPs. In addition, Pep-LNP-treated cells showed a much wider distribution of red fluorescent dots than those treated with nLNPs and PEG-LNPs. This further confirms that the intracellular delivery efficiency of Pep-LNPs is higher than that of nLNPs and PEG-LNPs. In contrast, more Cy3-siRNA in LNPs colocalized with LysoTracker Green in A549 cells than in Lipo2000 group (Fig. 3I), which may explain the compromised gene silencing effect on those cells (Fig. 3C and F).

3.4. LNPs promote the accumulation and extend the retention of siRNAs in the lung after pulmonary administration

Prior to evaluating the *in vivo* pharmacological effects of the LNPs, their biodistribution in various vital organs of mice following pulmonary administration were characterized using an IVIS imaging system. In addition, the retention of the LNPs-siRNA in the lung as a function of time was investigated.

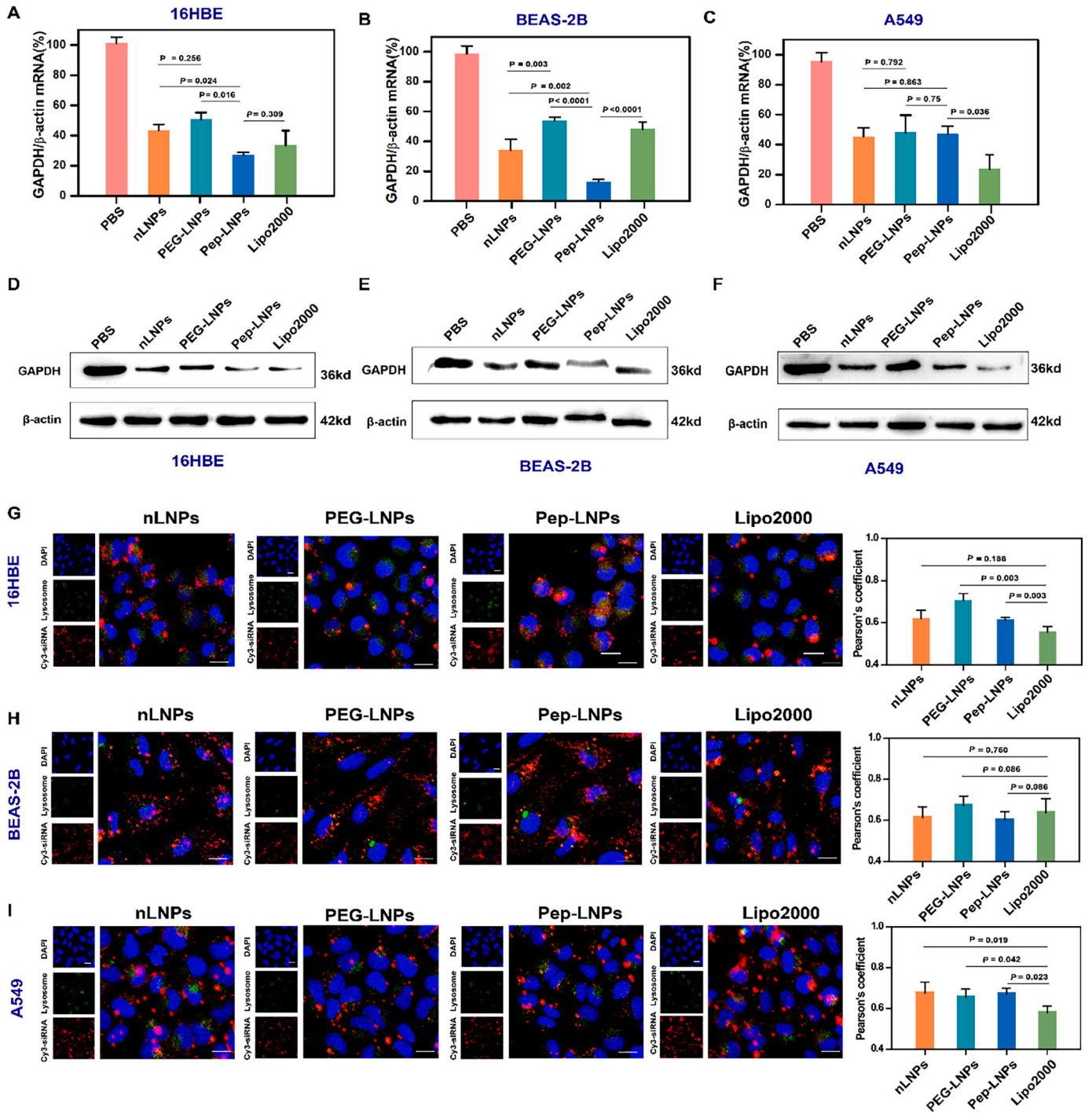

Fig. 3. *In vitro* gene silencing effects and endosome colocalization. Relative mRNA level based on RT–PCR (A-C) and protein expression level based on Western blot (D—F) in three cell lines (mean ± SD, $n = 3$). CLSM analysis of the intracellular localization of Cy3-siRNA-loaded LNPs (red) with endosomes and measurement of Pearson's coefficient in 16HBE (G), BEAS-2B (H) and A549 cells (I). The nucleus was stained with DAPI (blue), and lysosomes were stained with LysoTracker (green). Scale bar = 10 μm. (For interpretation of the references to colour in this figure legend, the reader is referred to the web version of this article.)

As shown in Fig. 4A, the LNPs-siRNA exhibited significantly greater accumulation in the lung than in the gastrointestinal (GI) tract, whereas no fluorescence signal was detected in other organs, such as the heart, liver, kidneys, and spleen, even 24 h after pulmonary administration. The fluorescence signals observed in the GI tract suggested that the LNPs might either be swallowed by the mice during intratracheal administration or underwent a mucociliary clearance in the airway followed by swallowing [55]. In contrast, in the free siRNA group, fluorescence signals were observed in the GI tract, liver, kidneys and spleen at 24 h after pulmonary administration. This suggests that free siRNA can translocate from the lung into the systemic circulation after administration. The encapsulation of siRNA in LNPs results in reduced translocation of siRNA molecules from the lung to systemic circulation. This might be accredited to the close association between siRNA and its vector, which prevents cargo leakage from the LNPs. In addition, the epithelial cell layers of lungs might have created a barrier for the LNPs to transport across the biomembrane and into the blood circulation. The limited systemic exposure of siRNA after its loading into nanocarriers

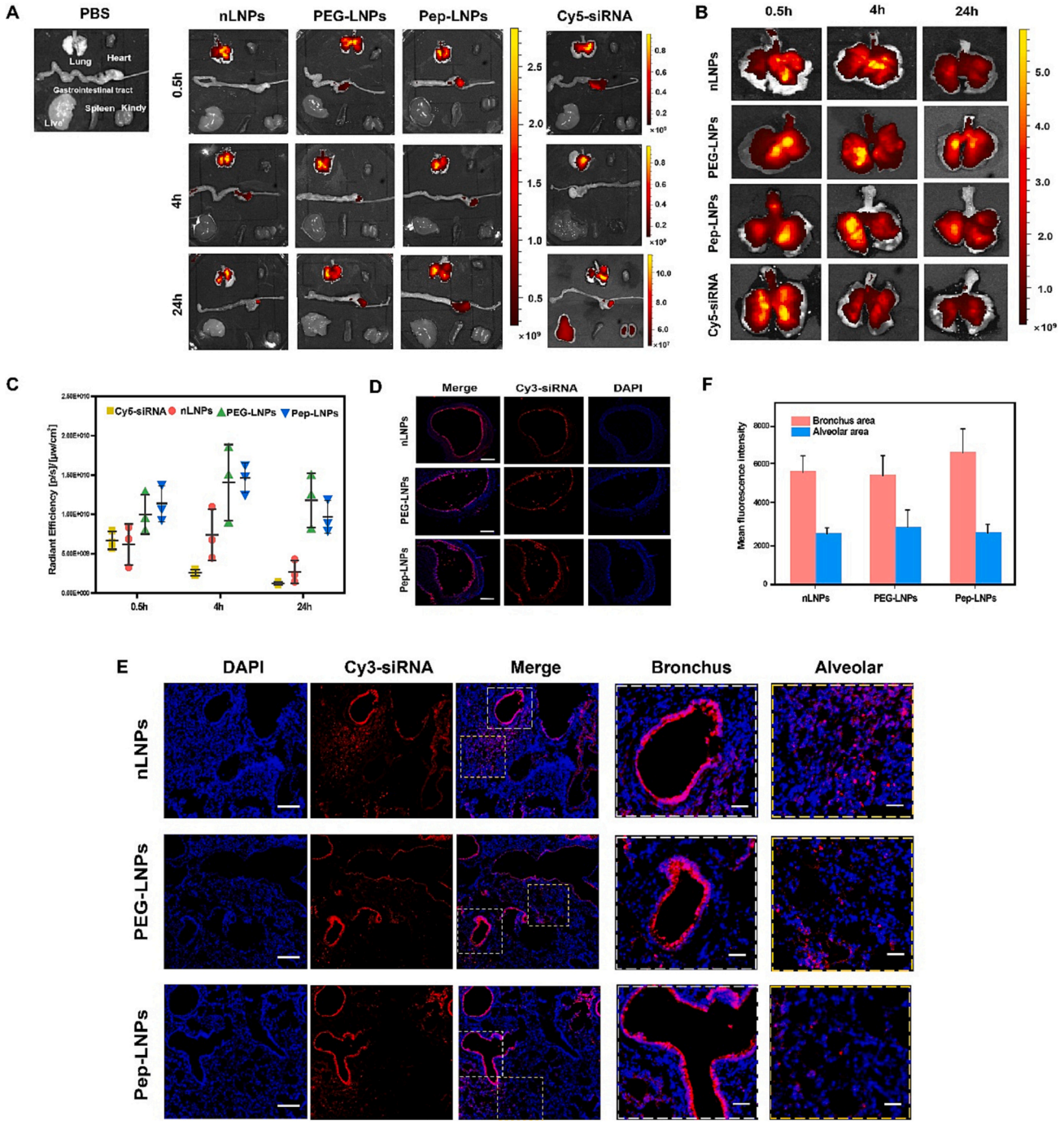

Fig. 4. Biodistribution and lung accumulation after pulmonary administration. Distribution in the vital organs of the animals at different time points after administration (A). Representative IVIS images of animal lungs harvested at variable time points after intratracheal administration (B). Radiant efficiency measured by IVIS for different animal groups over time (C) (mean ± SD, $n = 3$). Tracheal distribution of Cy3-siRNA-loaded LNPs 0.5 h after administration (D). LNPs-siRNA distribution in lung parenchyma 4 h after administration and the zoomed-in images showing the cellular localization of LNPs in bronchus and alveolar regions. Scale bar =100 μm (E). The mean fluorescence intensity (MFI) of Cy3-siRNA in the bronchus and alveolar areas was quantified using ImageJ software (MFI = Total fluorescence intensity in the region/the area of this region) (F) (mean ± SD, n = 3).

after pulmonary administration was also reported by other research groups [56].

Subsequently, *ex vivo* images of the lungs were collected, and the fluorescence intensities were quantified at 0.5, 4, and 24 h after pulmonary administration. As depicted in Fig. 4B and C, the fluorescence intensity of free Cy5-siRNA in the lungs decreased as a function of time, whereas the fluorescence signals from all the LNP treated groups remained obviously prominent even after 24 h of the administration. nLNPs exhibited comparatively lower fluorescence intensity in the lungs than PEG-LNPs and Pep-LNPs at all sampling points. These results indicate that loading siRNA into LNPs could prolong siRNA retention in the lungs. In addition, both PEGylation and surface modification with the peptide ligand could extend LNPs retention in mouse lungs [44].

To further confirm the extended lung retention and evaluate the airway distribution of the siRNA-loaded LNPs, the lung tissues were sliced with a cryo-microtome and observed by CLSM. We first observed the distribution of Cy3-siRNA-loaded LNPs in the trachea and upper airway, where mucus is abundant, and then the lung lobes [57]. The

LNPs were spread widely along the tracheal tract without obvious aggregation (Fig. 4D). There was no clear difference observed in the airway coverage of the fluorescence signals among nLNPs, PEG-LNPs, and Pep-LNPs. Airway mucin possess negatively-charged glycan coating and periodic hydrophobic domains, which can trap inhaled nanoparticles *via* electrostatic adherence and hydrophobic interactions [16,58]. We speculate that the mucus layer in the lungs of mice is too thin to trap these LNPs. Previous studies have also pointed out the limitations of mice models for evaluating the mucus penetration ability due to the species differences in emulating thick mucus layer in human airways [59]. It has been reported that PEGylation can promote the diffusion of nanoparticles in mucus *via* decreased hydrophobic and electrostatic interactions [58]. Therefore, PEG-LNPs was expected to show stronger mucus diffusion ability than that of nLNPs. To investigate the mucus penetration ability, we also developed *in vitro* mucus diffusion model according to the method reported in previous studies [60,61]. The result was shown in Fig. S6. Unexpectedly, we did not find significant differences in the mucus penetration ability among different LNP formulations. We reflected that airway mucus simulants in the diffusion model that can closely mimic *in vivo* physiological conditions of the disease lungs need to be further optimized to provide a solid basis for selection of the formulations [62].

The cryosections of the lung lobes demonstrated a higher fluorescence intensity in AECs along the bronchus than in the lower airways and alveoli (Fig. 4E and F). The colocalization of Cy3-siRNA-loaded LNPs (red) with the nuclei (blue) verified the efficient internalization of LNPs into the AECs across the airway [58]. The cellular internalization of the LNPs might result in the prolonged lung retention and lower systemic exposure, as mentioned above. However, considering the variability in the anatomic structure of the lungs, these sliced sections may not be able to reflect the cellular uptake throughout the whole lung tissue [63]. A quantitative method was therefore adopted to evaluate the cellular-level distribution of these LNPs within the lungs, and the results are presented in the following section.

3.5. Pep-LNPs enhanced siRNA delivery efficiency in AECs after pulmonary administration

To study the distribution of siRNA in the lung at cellular resolution, the fluorescence intensities of Cy5-siRNA-loaded LNPs in three types of lung cells, *i.e.*, Immune cells (ICs), endothelial cells (ECs) and epithelial cells (EpiCs) were determined at 8 h post pulmonary administration. The cell subsets of ICs (CD45 + CD31-), ECs (CD31 + CD45-), EpiCs (EpCAM+) and epithelial cells expressing ICAM-1 (*i.e.*, EpiC-ICAM-1, EpCAM+ICAM-1+) were identified (Fig. S7A and B) [27,35]. The percentages of Cy5-siRNA-positive (Cy5-siRNA+) cells within these cell populations and their fluorescence intensity were quantified by using multicolor flow cytometry in both normal and asthmatic mice (Fig. S7C and D).

As illustrated in Fig. 5A and B, different types of lung cells exhibited variable uptake behaviors toward LNPs-siRNA after pulmonary administration. In both normal and asthmatic mice, EpiCs had the highest cellular uptake of the inhaled LNPs-siRNA among the three cell types. The high percentage of Cy5-siRNA+ epithelial cells corresponded with the high localization of siRNA in the AECs in the frozen tissue sections (Fig. 4E and F). Previously, some researchers have also reported that nano-carriers loaded with nucleic acid exhibited a superior transfection efficiency in EpiCs than the other lung cell types following pulmonary administration [35]. However, when LNPs were designed for lung targeting *via* intravenous (*i.v.*) administration, they tended to exhibit a high transfection effect in lung endothelial cells [27]. This suggests that inhaled formulations render easier accessibility to EpiCs after pulmonary administration than other administration routes.

The ICs represented the second-highest population of Cy5-siRNA+ cells (5–10%) (Fig. 5A). Previous studies have revealed that LNPs administered intravenously have could favor a quick transfection in

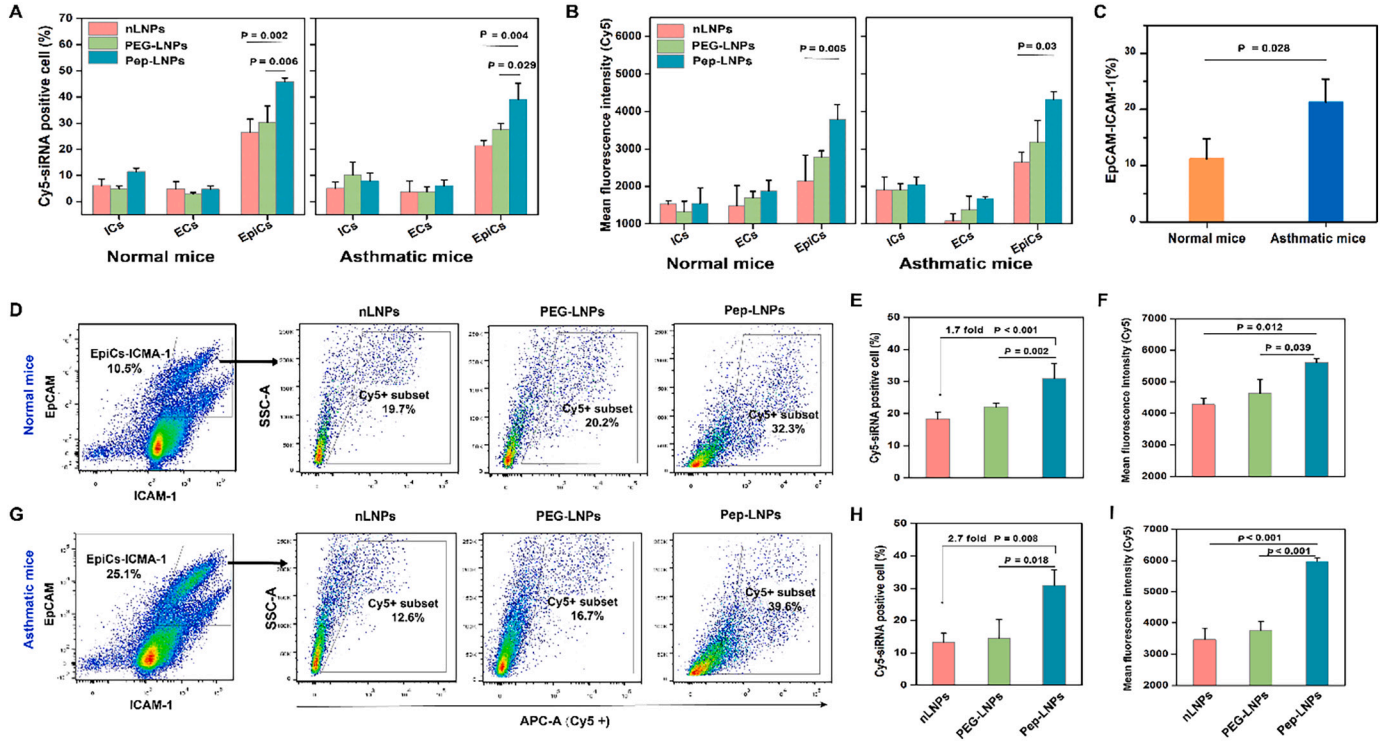

Fig. 5. Distribution of Cy5-siRNA-loaded LNPs in different cell populations in the lung tissue. Percentages of Cy5-siRNA+ cells (A) and MFI of Cy5-siRNA loaded LNPs (B) in different lung cell subsets of both normal and asthmatic mice (ICs, immune cells; ECs, endothelial cells; and EpiCs, epithelial cells). ICAM-1 expression levels in the epithelial cells of normal and asthmatic mice (C). The FACS analyses and their quantitative data of Cy5-siRNA+ cells and mean fluorescence intensity in epithelial cells populations expressing ICAM-1 (EpiCs-ICAM-1) in normal mice (D, E and F) and asthmatic mice (G, H and I) (mean ± SD, $n = 3$).

leukocytes [64]. Nevertheless, the LNPs prepared in our study depicted relatively limited uptake in immune cells, even under inflammatory conditions (*i.e.*, in asthmatic mice). Phagocytosis by macrophages is a known clearance pathway of inhaled nanoparticles, and the extent of phagocytosis is dependent on the physicochemical properties of the inhaled nanoparticles. Researchers have reported that positively charged particles are more readily phagocytosed by alveolar macrophages than negative or neutral-charged particles [65]. The neutrally charged surface of the LNPs might account for their low phagocytosis by immune cells. In addition to the surface charge, the size of the inhaled particles can also has a significant impact on phagocytosis by alveolar macrophages. Alveolar macrophages tend to phagocytose particles in the 1–5 μm size range. While particles >5 μm or with a diameter < 240 nm are less taken up by macrophages [65,66]. The nano-sizes of the LNPs in this study may also contribute to the results. Lastly, the favorable biocompatibility of the lipid components in the LNPs might be another important factor for the limited infiltration and phagocytosis of immune cells [67].

The percentage of Cy5-siRNA+ cells among the total endothelial cell population was negligible (<5%) (Fig. 5A). Endothelial cells showed very limited uptake of the inhaled LNPs-siRNA (Fig. 5A and B). These results confirm that the siRNA-loaded LNPs could hardly pass through the endothelial cells to reach to the blood system, which is in agreement with the IVIS imaging results.

Ligand incorporation has been considered an effective strategy for the selective delivery of nucleic acid-based therapeutics to the targeted cells [68,69]. For example, M. Kim and coworkers accomplished a targeted delivery of mRNA and siRNA to the liver sinusoidal endothelial cells by incorporating mannose moieties as ligand into LNPs [68]. Similarly, in our work, the peptide ligand-modified LNPs exhibited an enhanced delivery efficiency of siRNA to AECs expressing ICAM-1 (EpiCs-ICAM-1) compared to the other two formulations in both normal and asthmatic mice (Fig. 5D~I). In the normal mice, the delivery efficiency of Pep-LNPs in AECs expressing ICAM-1 was approximately 70% higher than that by nLNPs (Fig. 5D~F). Interestingly, in asthmatic mice, the delivery efficiency of Pep-LNPs n AECs expressing ICAM-1 was obvious enhanced, which was approximately 1.7-fold greater than that of nLNPs (Fig. 5G~I). This could be attributed to the higher expression level of ICAM-1 on the surface of AECs in asthmatic mice than normal mice (Fig. 5C). The enhanced expression of ICAM-1 in asthmatic airway epithelium has also been reported in literature [19,70]. The *in vivo* gene silencing effects of the LNPs were further evaluated at the protein level, and the results demonstrated that Pep-LNPs exhibited an improved gene silencing effect compared to the other two LNP formulations (Fig. S8).

3.6. Pep-LNPs-siTSLP alleviate airway inflammation and attenuate AHR

After confirming the AEC-specific siRNA delivery efficiency and enhanced gene silencing effects of Pep-LNPs, their therapeutic effects on asthmatic mice were investigated. In this context, TSLP-siRNA was loaded in Pep-LNPs and their abilities to alleviate inflammation and AHR were assessed in OVA-challenged allergic asthma mice after pulmonary administration (Fig. 6A). The epithelial-cell-derived cytokine, TSLP was targeted as it could regulate the multiple signaling pathways of the inflammatory cascades involved in the progression of asthma and acts as an alarmin for the immune system [12,13].

As shown in Fig. 6B, the total cell counts (including lymphocytes, eosinophils, macrophages, *etc.*) in the bronchoalveolar lavage fluid (BALF) of the asthmatic mice treated with PBS or Pep-LNPs-siNC were significantly higher than those of the Control group (*i.e.*, the mice sensitized and challenged by saline) or the mice treated with Pep-LNPs-siTSLP. However, there was no significant difference in the total number of cells between the Pep-LNP-siTSLP and Control groups. This trend remained unaltered in the case of percentages of lymphocytes and eosinophils (Fig. 6C and D). In contrast, the percentages of macrophages were higher in the Control group and mice treated with Pep-LNP-siTSLP compared to those treated with PBS and Pep-LNPs-siNC (Fig. 6E). This could be attributed to the fact that the percentages of macrophages were calculated rather than the absolute numbers of the cells, and similar results has been also reported in other studies [61,71]. Overall, these results imply that the total cell counts increased in the BALF of asthmatic mice, and Pep-LNP-siTSLP treatment could reduce the infiltration of eosinophils and lymphocytes in the airway, normalizing the total cell counts.

When looking into the cytokine levels, a significant increase in TSLP and Th2 cytokines (IL-4 and IL-13) in the BALF was observed in the mice treated with PBS compared to the Control group (Fig. 6F~H). In contrast, Pep-LNP-siTSLP-treated mice exhibited a significant decrease in the levels of TSLP, IL-4 and IL-13 in the BALF as compared to the PBS group ($p < 0.05$), and these cytokines levels in the Pep-LNP-siTSLP group were comparable to those in the Control group (Fig. 6F~H). A similar TSLP level in the mice treated with Pep-LNP-siNC and PBS suggested that Pep-LNPs-siNC did not exert an RNAi effect (Fig. 6F). The levels of IL-4 and IL-13 were determined in this study because TSLP is known to regulate the expression of several Th2 cytokines, including IL-4 and IL-13 [12,13,72]. It has been reported that IL-4 is involved in early allergic inflammation, activating various immune cells and elevating IgE levels [18], and IL-13 increases bronchus hyperactivity, promotes goblet cell hyperplasia and activates MUC5AC expression, which further contributes to the aggravation of airway obstruction [73,74].

TSLP and IL-13 are known to inhibit mucus overproduction, which is one of the remarkable pathological characteristics of asthma [75]. Therefore, to further evaluate the therapeutic effect caused by the suppression of TSLP and IL-13, the level of mucin MUC5AC in the lungs was determined by using both ELISA and Western blotting. As shown in Fig. 6 I and J, the expression levels of MUC5AC in asthmatic mice treated with PBS and Pep-LNPs-siNC were noticeably elevated compared with those in the Control group. Following the treatment with Pep-LNPs-siTSLP, the MUC5AC level in the BALF as determined by ELISA (Fig. 6I) and MUC5AC protein expression in lung tissues as analyzed by Western blotting (Fig. 6J) were significantly suppressed, conferring their abilities to reduce mucus overproduction.

The impact of attenuated expression of MUC5AC by Pep-LNPs-siTSLP treatment on lung functions was also evaluated by monitoring airway responsiveness in response to the variable concentration of aerosolized methacholine (Mch) [37,74]. The enhanced pause (Penh) was measured by whole-body plethysmography as an indicator of AHR. As shown in Fig. 6K, the starting Penh values (*i.e.*, baseline) of the various groups were almost the same and increased with raising concentration of Mch. The Penh values for the mice treated with PBS or Pep-LNPs-siNC increased to a much greater extent than those of the Control group. In contrast, the increase in the Penh values of the mice treated with Pep-LNPs-siTSLP as a function of Mch concentration remained comparable to that in the Control group. This indicated that Pep-LNPs-siTSLP treatment was able to protect the asthmatic airway from the stimulation by Mch and alleviate AHR. The outcomes could be supported by the H&E and PAS staining images (Fig. 6L and M). Pep-LNPs-siTSLP treatment resulted in less inflammatory cell infiltration both in the peribronchial and alveolar areas of asthmatic lungs than PBS or Pep-LNPs-siNC treatment (Fig. 6L). In addition, Pep-LNPs-siTSLP treatment prevented the hyperplasia of PAS positive cells, which was obvious in the groups treated with PBS and Pep-LNPs-siNC (Fig. 6M). These results suggested that Pep-LNPs-siTSLP could be a promising therapy to alleviate epithelium-mediated inflammatory responses and attenuate AHR in the asthmatic conditions.

3.7. Pep-LNPs are well tolerated by mice after pulmonary administration

The safety profiles of the LNPs-siRNA after pulmonary administration to healthy mice were assessed and compared with lipopolysaccharide (LPS) (*i.e.,* positive control) by quantifying the proinflammatory cytokines in the BALF, counting the infiltrated inflammatory cells, and

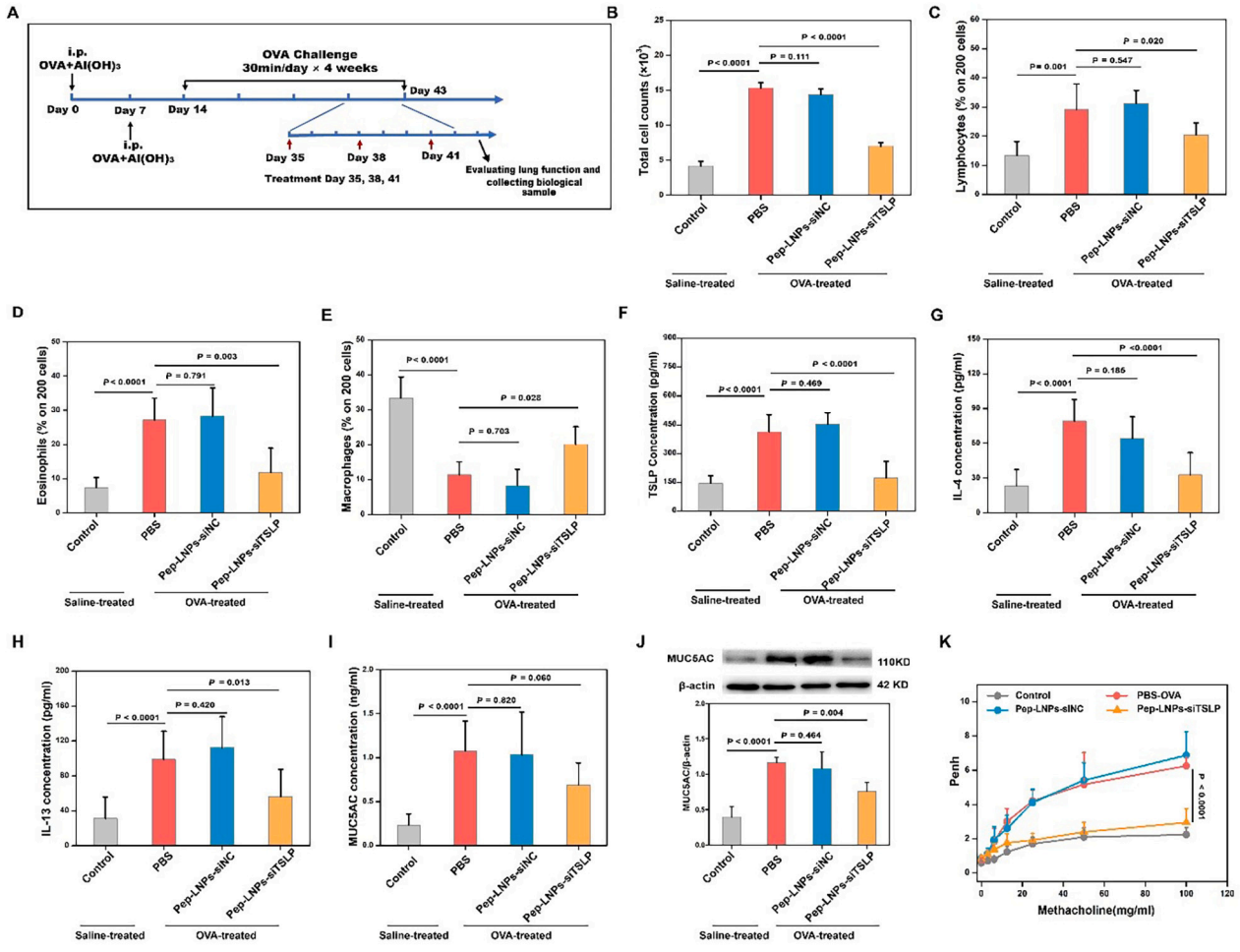

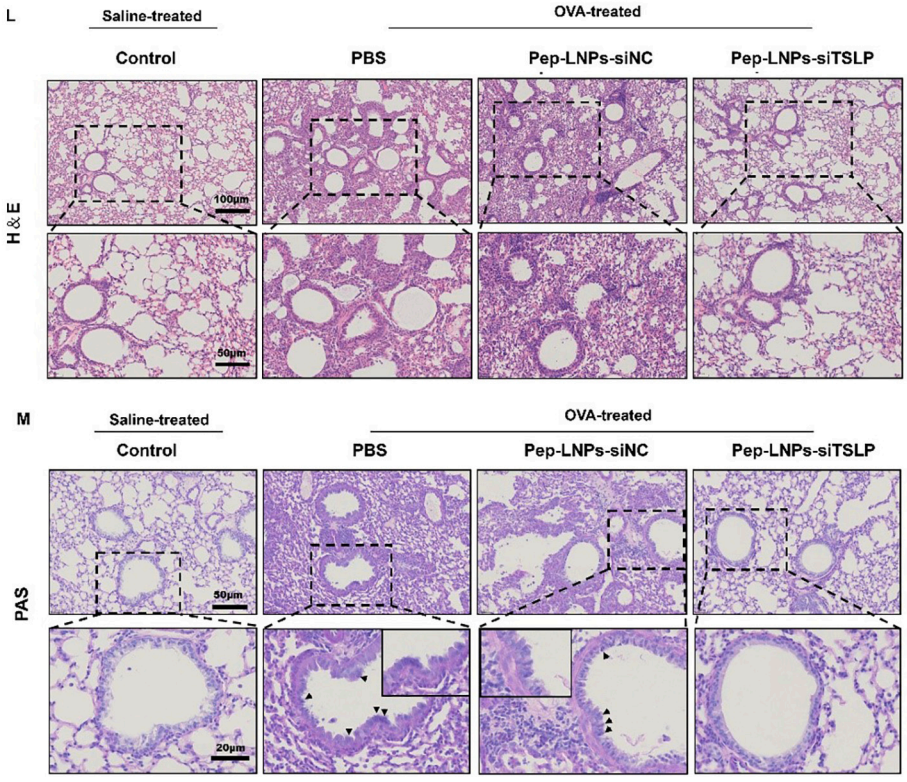

(caption on next page)

Fig. 6. Illustration of the asthma model development and treatment protocol (A). Total cell counts and the percentages of lymphocytes, eosinophils, and macrophages in the BALF (B-E). TSLP (F), IL-4 (G), IL-13 (H) and MUC5AC (I) levels in the BALF determined by ELISA. MUC5AC expression in the lung tissue determined by Western blot (J). Airway responsiveness in response to increasing doses of Mch ($n = 6$) (K). Representative images of H&E staining (L) demonstrating inflammatory cell infiltration. PAS staining of the lung sections after various treatments (M) demonstrating mucus-producing PAS-positive cells (dark purple). Scale bar: 100 μm for 200×, 50 μm for 400×. (mean ± SD, n = 6, * $p < 0.05$, ** $p < 0.01$, *** $p < 0.001$, *ns*, no significance). (For interpretation of the references to colour in this figure legend, the reader is referred to the web version of this article.)

H&E staining. LPS is outer membrane component of Gram-negative bacteria and known as a strong stimulator of innate or natural immunity [76]. As illustrated in Fig. 7A~C, the levels of IL-1β, IL-6, and TNF-α in the mice treated with the LNPs were comparable with those in the PBS group, whereas the mice treated with LPS demonstrated significantly higher levels of these proinflammatory cytokines. The high levels of these proinflammatory cytokines could initiate the production of inflammatory mediators, trigger the immune response, and induce epithelial cell injury [77–79].

There were no significant differences in the total cell counts between PBS group and the LNP groups. In contrast, the total cell counts for the mice treated with LPS increased dramatically compared to the PBS group (Fig. 7D). Generally, macrophages account for most of the cells in BALF, and other immune cells make up a small proportion in normal mice [80]. As depicted in Fig. 7E, the percentages of neutrophils in the BALF of the mice treated with the LNP formulations were comparable to

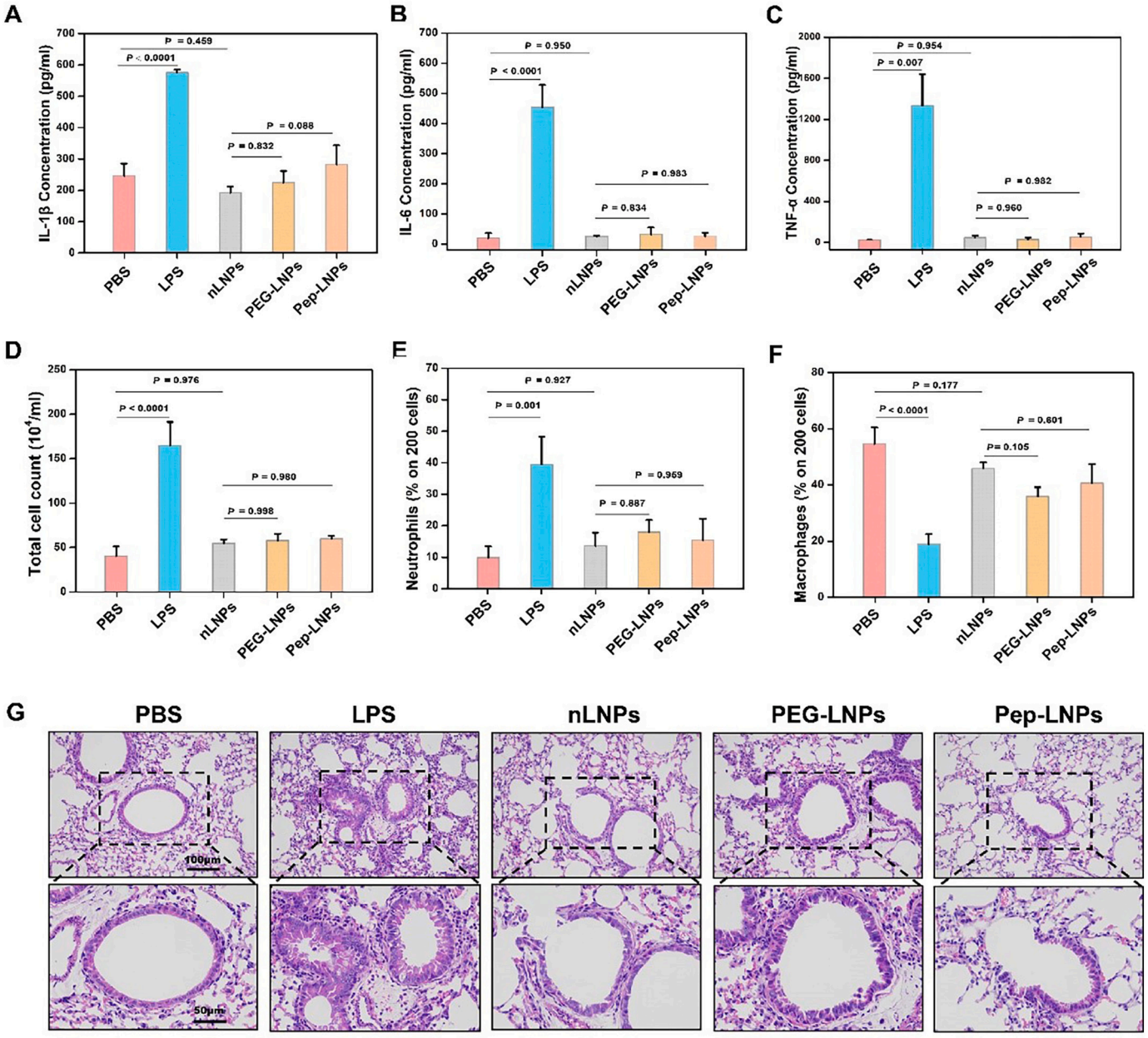

Fig. 7. Safety assessment of LNPs-siRNA (siNC) and LPS after intratracheal administration. Inflammatory cytokines in BALF determined by ELISA (A-C), total cell counts (D) and the percentages of neutrophils (E) and macrophages (F) in BALF (mean ± SD, $n = 3$). Representative histology images of the lung tissue by H&E staining (G). Scale bar: 100 μm (200×), 50 μm (400×).

those treated with PBS, whereas a notable increase in the percentage of neutrophils was observed in the mice treated with LPS. The proportion of macrophages in the BALF was lower in the LPS group than in the PBS and LNPs treated groups (Fig. 7F). Thus, LPS treatment could induce neutrophil infiltration and relatively reduce the proportion of macrophages [61]. These results suggest that LPS treatment, but not the LNP formulations, resulted in significant inflammatory cell infiltration in the airway.

To further understand the histopathological changes in lung tissues, H&E staining was performed and analyzed using a light microscope. The H&E staining images of lungs from PBS-treated mice displayed clear alveoli spaces and normal bronchial walls, without inflammatory cell infiltration (Fig. 7 G). In contrast, noticeable inflammatory cell infiltration in the interstitial and alveolar spaces and thickened airway cavity walls were observed in the mice treated with LPS. The histological features of the LNPs treated groups were similar to those of the mice treated with PBS, no obvious inflammatory lesions were observed in both airway and alveolar region. These results suggested that the LNPs could be well tolerated in mice without obvious lung inflammation or toxicity under the dosage regimen in this work.

4. Conclusion

In summary, cyclic peptide-decorated lipid nanoparticles (Pep-LNPs) were successfully accomplished, which could efficiently deliver siRNA into cultured human epithelial cells and mouse AECs and markedly reduce the expression of TSLP, a proinflammatory cytokine that sits at the top of the inflammatory cascade. The inhibition of TSLP by the Pep-LNPs regulated multiple signaling pathways (*i.e.*, IL-4 and IL-13) involved in the progression of asthma, which subsequently reduced stimulated MUC5AC secretion and alleviated the inflammatory response and AHR. In addition, the Pep-LNPs showed a very low rate of immunogenicity when administered intratracheally, so this is unlikely to be a limitation of chronic therapy. Pep-LNPs might therefore serve as a promising therapy in controlling acute exacerbation of asthma and could also be used to treat patients suffering from poor control of mucus hypersecretion by modulating upstream inflammatory mediators. Altogether, this study demonstrates that the inhaled ionizable lipid nanoparticles are an effective and safe delivery platform against proinflammatory genes overexpressed in AECs. In view of the complex pathogenesis of asthma, our research may also pave the way for the delivery of cocktail siRNAs targeting various genes overexpressed in AECs to develop therapeutics with synergistic pharmacological effects.

CRediT authorship contribution statement

Mengjun Zhang: Methodology, Formal analysis, Investigation, Writing – original draft. **Huiyang Jiang:** Investigation. **Lan Wu:** Methodology, Writing – review & editing. **Haoyu Lu:** Investigation. **Hriday Bera:** Writing – review & editing, Visualization. **Xing Zhao:** Investigation. **Xiong Guo:** Formal analysis, Visualization. **Xulu Liu:** Investigation. **Dongmei Cun:** Supervision, Methodology, Writing – review & editing. **Mingshi Yang:** Conceptualization, Funding acquisition, Supervision, Writing – review & editing.

Declaration of Competing Interest

The authors declare no conflicts of interest in this work.

Data availability

Data will be made available on request.

Acknowledgements

This work was financially supported by the Liaoning Pan Deng Xue Zhe Scholar (No. XLYC2002061), the National Natural Science Foundation of China (No. 82173768), and the Overseas Expertise Introduction Project for Discipline Innovation ("111 Project") (No. D20029). L. W. acknowledges the financial supports from National Natural Science Foundation of China, Govt. of China (grant No. 82204316) and China Postdoctoral Science Foundation, Govt. of China (grant No. 2021TQ0219 and 2022MD713776). H.B. thanks the financial support from National Natural Science Foundation of China, Govt. of China (grant No. 81850410554 and 82050410448) and Fellowship of China Postdoctoral Science Foundation, Govt. of China (grant No. 2021MD703857). X.G. acknowledges the 2021 annual scientific research funding project of the Educational Department of Liaoning Province (grant No. LJKZ0925) and higher education institutions fundamental scientific research project of the Educational Department of Liaoning Province (Youth Project, grant No. LJKQZ2021035). D.C. acknowledges financial support from Provincial Natural Science Foundation Project of Liaoning (NO. 2022-MS-241), General program of Provincial Department of Education of Liaoning (NO. LJKZ0951) and Liaoning Xingliao Young Top Talent (NO. XLYC1907042).

References

[1] S.A. Heialy, R.K. Ramakrishnan, Q. Hamid, Recent advances in the immunopathogenesis of severe asthma, J. Allergy Clin. Immunol. 149 (2022) 455–465.
[2] M. E, The Global Asthma Report. http://www.globalasthmareport.org, 2018.
[3] H. Lee, J. Ryu, E. Nam, S.J. Chung, Y. Yeo, D.W. Park, T.S. Park, J.-Y. Moon, T.-H. Kim, J.W. Sohn, H.J. Yoon, S.-H. Kim, Increased mortality in patients with corticosteroid-dependent asthma: a nationwide population-based study, Eur. Respir. J. 54 (2019) 1900804.
[4] P.J. Barnes, Corticosteroid resistance in patients with asthma and chronic obstructive pulmonary disease, J. Allergy Clin. Immunol. 131 (2013) 636–645.
[5] H.H.F. Tang, S.M. Teo, P.D. Sly, P.G. Holt, M. Inouye, The intersect of genetics, environment, and microbiota in asthma—perspectives and challenges, J. Allergy Clin. Immunol. 147 (2021) 781–793.
[6] S.P. Sajuthi, J.L. Everman, N.D. Jackson, B. Saef, C.L. Rios, C.M. Moore, A.C. Y. Mak, C. Eng, A. Fairbanks-Mahnke, S. Salazar, J. Elhawary, S. Huntsman, V. Medina, D.A. Nickerson, S. Germer, M.C. Zody, G. Abecasis, H.M. Kang, K. M. Rice, R. Kumar, N.A. Zaitlen, S. Oh, J. Rodríguez-Santana, E.G. Burchard, M. A. Seibold, N.T.-O.f.P.M. Consortium, Nasal airway transcriptome-wide association study of asthma reveals genetically driven mucus pathobiology, Nat. Commun. 13 (2022) 1632.
[7] M. Kudo, Y. Ishigatsubo, I. Aoki, Pathology of asthma, Front. Microbiol. 4 (2013).
[8] Y. Yang, M. Jia, Y. Ou, I.M. Adcock, X. Yao, Mechanisms and biomarkers of airway epithelial cell damage in asthma: a review, Clin. Respir. J. 15 (10) (2021) 1027–1045.
[9] B. Hu, L. Zhong, Y. Weng, L. Peng, Y. Huang, Y. Zhao, X.-J. Liang, Therapeutic siRNA: state of the art, Signal Transd. Targeted Ther. 5 (2020) 101.
[10] K. Dua, R. Wadhwa, G. Singhvi, V. Rapalli, S.D. Shukla, M.D. Shastri, G. Gupta, S. Satija, M. Mehta, N. Khurana, R. Awasthi, P.K. Maurya, L. Thangavelu, M. M. Tambuwala, T. Collet, P.M. Hansbro, D.K. Chellappan, The potential of siRNA based drug delivery in respiratory disorders: recent advances and progress, Drug Dev. Res. 80 (2019) 714–730.
[11] Y. Xu, A. Thakur, Y. Zhang, C. Foged, Inhaled RNA therapeutics for obstructive airway diseases: recent advances and future prospects, Pharmaceutics 13 (2021) 177.
[12] V. Soumelis, Y.-J. Liu, The discovery of human TSLP as a critical epithelial cytokine in type 2 immunity and allergic disease, Nat. Immunol. 21 (2020) 1471–1473.
[13] B. Zhou, M.R. Comeau, T.D. Smedt, H.D. Liggitt, M.E. Dahl, D.B. Lewis, D. Gyarmati, T. Aye, D.J. Campbell, S.F. Ziegler, Thymic stromal lymphopoietin as a key initiator of allergic airway inflammation in mice, Nat. Immunol. 6 (2005) 1047–1053.
[14] G.M. Gauvreau, P.M. O'Byrne, L.-P. Boulet, Y. Wang, D. Cockcroft, J. Bigler, J. M. FitzGerald, M. Boedigheimer, B.E. Davis, C. Dias, K.S. Gorski, L. Smith, E. Bautista, M.R. Comeau, R. Leigh, J.R. Parnes, Effects of an anti-TSLP antibody on allergen-induced asthmatic responses, N. Engl. J. Med. 370 (2014) 2102–2110.
[15] C. Shaffer, Mist begins to clear for lung delivery of RNA, Nat. Biotechnol. 38 (2020) 1110–1113.
[16] L. Ding, S. Tang, T.A. Wyatt, D.L. Knoell, D. Oupický, Pulmonary siRNA delivery for lung disease: review of recent progress and challenges, J. Control. Release 330 (2021) 977–991.
[17] M.Y.T. Chow, Y. Qiu, J.K.W. Lam, Inhaled RNA therapy: from promise to reality, Trends Pharmacol. Sci. 41 (2020) 715–729.
[18] H. Hammad, B.N. Lambrecht, The basic immunology of asthma, Cell 184 (2021) 1469–1485.
[19] D. Blaas, R. Fuchs, Mechanism of human rhinovirus infections, Mol. Cell. Pediatr. 3 (2016) 21.

[20] J.M. Greve, G. Davis, A.M. Meyer, C.P. Forte, S.C. Yost, C.W. Marlor, M. E. Kamarck, A. McClelland, The major human rhinovirus receptor is ICAM-1, Cell 56 (1989) 839–847.
[21] A.M. Vignola, A.M. Campbell, P. Chanez, J. Bousquet, P. Paul-Lacoste, F.-B. Michel, P. Godard, HLA-DR and ICAM-1 expression on bronchial epithelial cells in asthma and chronic bronchitis, Am. Rev. Respir. Dis. 148 (1993) 689–694.
[22] D.E. Parry, W.W. Busse, K.A. Sukow, C.R. Dick, C. Swenson, J.E. Gern, Rhinovirus-induced PBMC responses and outcome of experimental infection in allergic subjects, J. Allergy Clin. Immunol. 105 (2000) 692–698.
[23] A.D. Tagalakis, R.J. McAnulty, J. Devaney, S.E. Bottoms, J.B. Wong, M. Elbs, M. J. Writer, H.C. Hailes, A.B. Tabor, C. O'Callaghan, A. Jaffe, S.L. Hart, A receptor-targeted nanocomplex vector system optimized for respiratory gene transfer, Mol. Ther. 16 (2008) 907–915.
[24] C. Garnacho, R. Dhami, M. Solomon, E.H. Schuchman, S. Muro, Enhanced delivery and effects of acid sphingomyelinase by ICAM-1-targeted nanocarriers in type B Niemann-pick disease mice, Mol. Ther. 25 (2017) 1686–1696.
[25] A. Akinc, M.A. Maier, M. Manoharan, K. Fitzgerald, M. Jayaraman, S. Barros, S. Ansell, X. Du, M.J. Hope, T.D. Madden, B.L. Mui, S.C. Semple, Y.K. Tam, M. Ciufolini, D. Witzigmann, J.A. Kulkarni, R. van der Meel, P.R. Cullis, The Onpattro story and the clinical translation of nanomedicines containing nucleic acid-based drugs, Nat. Nanotechnol. 14 (2019) 1084–1087.
[26] E. Samaridou, J. Heyes, P. Lutwyche, Lipid nanoparticles for nucleic acid delivery: current perspectives, Adv. Drug Deliv. Rev. 154-155 (2020) 37–63.
[27] Q. Cheng, T. Wei, L. Farbiak, L.T. Johnson, S.A. Dilliard, D.J. Siegwart, Selective organ targeting (SORT) nanoparticles for tissue-specific mRNA delivery and CRISPR–Cas gene editing, Nat. Nanotechnol. 15 (2020) 313–320.
[28] M.J. Writer, B. Marshall, M.A. Pilkington-Miksa, S.E. Barker, M. Jacobsen, A. Kritz, P.C. Bell, D.H. Lester, A.B. Tabor, H.C. Hailes, N. Klein, S.L. Hart, Targeted gene delivery to human airway epithelial cells with synthetic vectors incorporating novel targeting peptides selected by phage display, J. Drug Target. 12 (2004) 185–193.
[29] M.K. Shim, Y. Moon, S. Yang, J. Kim, H. Cho, S. Lim, H.Y. Yoon, J.-K. Seong, K. Kim, Cancer-specific drug-drug nanoparticles of pro-apoptotic and cathepsin B-cleavable peptide-conjugated doxorubicin for drug-resistant cancer therapy, Biomaterials 261 (2020), 120347.
[30] L.B. Jeffs, L.R. Palmer, E.G. Ambegia, C. Giesbrecht, S. Ewanick, I. MacLachlan, A. Scalable, Extrusion-free method for efficient liposomal encapsulation of plasmid DNA, Pharm. Res. 22 (2005) 362–372.
[31] J.A. Kulkarni, P.R. Cullis, R. van der Meel, Lipid nanoparticles enabling gene therapies: from concepts to clinical utility, Nucleic Acid Ther. 28 (2018) 146–157.
[32] J.-B. Qiao, Q.-Q. Fan, C.-L. Zhang, J. Lee, J. Byun, L. Xing, X.-D. Gao, Y.-K. Oh, H.-L. Jiang, Hyperbranched lipoid-based lipid nanoparticles for bidirectional regulation of collagen accumulation in liver fibrosis, J. Control. Release 321 (2020) 629–640.
[33] K.J. Livak, T.D. Schmittgen, Analysis of relative gene expression data using real-time quantitative PCR and the $2-\Delta\Delta CT$ method, Methods 25 (2001) 402–408.
[34] R.K. Kumar, C. Herbert, P.S. Foster, The "classical" ovalbumin challenge model of asthma in mice, Curr. Drug Targets 9 (2008) 485–494.
[35] A.K. Patel, J.C. Kaczmarek, S. Bose, K.J. Kauffman, F. Mir, M.W. Heartlein, F. DeRosa, R. Langer, D.G. Anderson, Inhaled nanoformulated mRNA polyplexes for protein production in lung epithelium, Adv. Mater. 31 (2019) 1805116.
[36] L. Sun, M. Fan, D. Huang, B. Li, R. Xu, F. Gao, Y. Chen, Clodronate-loaded liposomal and fibroblast-derived exosomal hybrid system for enhanced drug delivery to pulmonary fibrosis, Biomaterials 271 (2021), 120761.
[37] W. Pei, X. Li, R. Bi, X. Zhang, M. Zhong, H. Yang, Y. Zhang, K. Lv, Exosome membrane-modified M2 macrophages targeted nanomedicine: treatment for allergic asthma, J. Control. Release 338 (2021) 253–267.
[38] Y.-L. Chen, B.-L. Chiang, Targeting TSLP with shRNA alleviates airway inflammation and decreases epithelial CCL17 in a murine model of asthma, Mol. Ther. Nucl. Acids 5 (2016), e316.
[39] I.H. Heijink, V.N.S. Kuchibhotla, M.P. Roffel, T. Maes, D.A. Knight, I. Sayers, M. C. Nawijn, Epithelial cell dysfunction, a major driver of asthma development, Allergy 75 (2020) 1902–1917.
[40] S. Zafar, S. Beg, S.K. Panda, M. Rahman, K.S. Alharbi, G.K. Jain, F.J. Ahmad, Novel therapeutic interventions in cancer treatment using protein and peptide-based targeted smart systems, Semin. Cancer Biol. 69 (2021) 249–267.
[41] J. Leal, X. Peng, X. Liu, D. Arasappan, D.C. Wylie, S.H. Schwartz, J.J. Fullmer, B. C. McWilliams, H.D.C. Smyth, D. Ghosh, Peptides as surface coatings of nanoparticles that penetrate human cystic fibrosis sputum and uniformly distribute in vivo following pulmonary delivery, J. Control. Release 322 (2020) 457–469.
[42] A. Chakraborty, A.A. Pinar, M. Lam, J.E. Bourke, S.G. Royce, C. Selomulya, C. S. Samuel, Pulmonary myeloid cell uptake of biodegradable nanoparticles conjugated with an anti-fibrotic agent provides a novel strategy for treating chronic allergic airways disease, Biomaterials 273 (2021), 120796.
[43] C.A. Alabi, K.T. Love, G. Sahay, T. Stutzman, W.T. Young, R. Langer, D. G. Anderson, FRET-labeled siRNA probes for tracking assembly and disassembly of siRNA Nanocomplexes, ACS Nano 6 (2012) 6133–6141.
[44] T. Chen, B. He, J. Tao, Y. He, H. Deng, X. Wang, Y. Zheng, Application of Förster resonance energy transfer (FRET) technique to elucidate intracellular and in vivo biofate of nanomedicines, Adv. Drug Deliv. Rev. 143 (2019) 177–205.
[45] V. Francia, R.M. Schiffelers, P.R. Cullis, D. Witzigmann, The biomolecular Corona of lipid nanoparticles for gene therapy, Bioconjug. Chem. 31 (2020) 2046–2059.
[46] S. Boero, M. Silvestri, N. Ullmann, G.A. Rossi, Modulation by Flunisolide of tumor necrosis factor-α–induced stimulation of airway epithelial cell activities related to eosinophil inflammation, J. Asthma 47 (2010) 381–387.
[47] S.C.H. Chan, D.K.Y. Shum, G.L. Tipoe, J.C.W. Mak, E.T.M. Leung, M.S.M. Ip, Upregulation of ICAM-1 expression in bronchial epithelial cells by airway secretions in bronchiectasis, Respir. Med. 102 (2008) 287–298.
[48] D. Sanmugalingam, A.J. Wardlaw, P. Bradding, Adhesion of human lung mast cells to bronchial epithelium: evidence for a novel carbohydrate-mediated mechanism, J. Leukoc. Biol. 68 (2000) 38–46.
[49] R. Ghanem, V. Laurent, P. Roquefort, T. Haute, S. Ramel, T. Le Gall, T. Aubry, T. Montier, Optimizations of in vitro mucus and cell culture models to better predict in vivo gene transfer in pathological lung respiratory airways: cystic fibrosis as an example, Pharmaceutics 13 (2021) 47.
[50] B.L. Mui, Y.K. Tam, M. Jayaraman, S.M. Ansell, X. Du, Y.Y.C. Tam, P.J.C. Lin, S. Chen, J.K. Narayanannair, K.G. Rajeev, M. Manoharan, A. Akinc, M.A. Maier, P. Cullis, T.D. Madden, M.J. Hope, Influence of polyethylene glycol lipid desorption rates on pharmacokinetics and pharmacodynamics of siRNA lipid nanoparticles, Mol. Ther. Nucl. Acids 2 (2013), e139.
[51] S. Mishra, P. Webster, M.E. Davis, PEGylation significantly affects cellular uptake and intracellular trafficking of non-viral gene delivery particles, Eur. J. Cell Biol. 83 (2004) 97–111.
[52] X. Liang, J. Zhang, H. Ou, J. Chen, S. Mitragotri, M. Chen, Skin delivery of siRNA using sponge spicules in combination with cationic flexible liposomes, Mol. Ther. Nucl. Acids 20 (2020) 639–648.
[53] D.P. Feldmann, Y. Cheng, R. Kandil, Y. Xie, M. Mohammadi, H. Harz, A. Sharma, D. J. Peeler, A. Moszczynska, H. Leonhardt, S.H. Pun, O.M. Merkel, In vitro and in vivo delivery of siRNA via VIPER polymer system to lung cells, J. Control. Release 276 (2018) 50–58.
[54] Y. Qiu, M. Clarke, L.T.L. Wan, J.C.K. Lo, A.J. Mason, J.K.W. Lam, Optimization of PEGylated KL4 peptide for siRNA delivery with improved pulmonary tolerance, Mol. Pharm. 18 (2021) 2218–2232.
[55] L. Wu, C. Rodríguez-Rodríguez, D. Cun, M. Yang, K. Saatchi, U.O. Häfeli, Quantitative comparison of three widely-used pulmonary administration methods in vivo with radiolabeled inhalable nanoparticles, Eur. J. Pharm. Biopharm. 152 (2020) 108–115.
[56] S. Haque, O. Feeney, E. Meeusen, B.J. Boyd, M.P. McIntosh, C.W. Pouton, M. Whittaker, L.M. Kaminskas, Local inflammation alters the lung disposition of a drug loaded pegylated liposome after pulmonary dosing to rats, J. Control. Release 307 (2019) 32–43.
[57] X. Huang, J. Chisholm, J. Zhuang, Y. Xiao, G. Duncan, X. Chen, J.S. Suk, J. Hanes, Protein nanocages that penetrate airway mucus and tumor tissue, Proc. Natl. Acad. Sci. 114 (2017) E6595–E6602.
[58] E. Robinson, K.D. MacDonald, K. Slaughter, M. McKinney, S. Patel, C. Sun, G. Sahay, Lipid nanoparticle-delivered chemically modified mRNA restores chloride secretion in cystic fibrosis, Mol. Ther. 26 (2018) 2034–2046.
[59] G. Osman, J. Rodriguez, S.Y. Chan, J. Chisholm, G. Duncan, N. Kim, A.L. Tatler, K. M. Shakesheff, J. Hanes, J.S. Suk, J.E. Dixon, PEGylated enhanced cell penetrating peptide nanoparticles for lung gene therapy, J. Control. Release 285 (2018) 35–45.
[60] S. Currie, S. Kim, X.C. Gu, X.O. Ren, F. Lin, S.X. Liu, C.B. Yang, J.H. Kim, S. Liu, Mucus-penetrating PEGylated polysuccinimide-based nanocarrier for intravaginal delivery of siRNA battling sexually transmitted infections, Colloids Surf. B: Biointerfaces 196 (2020) 111287–111298.
[61] Z. Li, G. Luo, W.P. Hu, J.L. Hua, S. Geng, P.K. Chu, J. Zhang, H. Wang, X.F. Yu, Mediated drug release from nanovehicles by black phosphorus quantum dots for efficient therapy of chronic obstructive pulmonary disease, Angew. Chem. 132 (2020) 20749.
[62] R. Ghanem, V. Laurent, P. Roquefort, T. Haute, S. Ramel, T. Le Gall, T. Aubry, T. Montier, Optimizations of in vitro mucus and cell culture models to better predict in vivo gene transfer in pathological lung respiratory airways: cystic fibrosis as an example, Pharmaceutics 13 (2021) 47–71.
[63] J.C. Mejías, K. Roy, In-vitro and in-vivo characterization of a multi-stage enzyme-responsive nanoparticle-in-microgel pulmonary drug delivery system, J. Control. Release 316 (2019) 393–403.
[64] S. Ramishetti, I. Hazan-Halevy, R. Palakuri, S. Chatterjee, S. Naidu Gonna, N. Dammes, I. Freilich, L. Kolik Shmuel, D. Danino, D. Peer, A combinatorial library of lipid nanoparticles for RNA delivery to leukocytes, Adv. Mater. 32 (2020) 1906128.
[65] Q. Liu, J. Guan, L. Qin, X. Zhang, S.R. Mao, Physicochemical properties affecting the fate of nanoparticles in pulmonary drug delivery, Drug Discov. Today 25 (2020) 150–159.
[66] Y. He, Y. Liang, R. Han, W.-L. Lu, J.C.W. Mak, Y. Zheng, Rational particle design to overcome pulmonary barriers for obstructive lung diseases therapy, J. Control. Release 314 (2019) 48–61.
[67] A.K. Patel, J.C. Kaczmarek, S. Bose, K.J. Kauffman, F. Mir, M.W. Heartlein, F. DeRosa, R. Langer, D.G. Anderson, Inhaled Nanoformulated mRNA Polyplexes for protein production in lung epithelium, Adv. Mater. 31 (2019) 1805116.
[68] M. Kim, M. Jeong, S. Hur, Y. Cho, J. Park, H. Jung, Y. Seo, H.A. Woo, K.T. Nam, K. Lee, H. Lee, Engineered ionizable lipid nanoparticles for targeted delivery of RNA therapeutics into different types of cells in the liver, Sci. Adv. 7 (2021) eabf4398.
[69] J. Zhang, H. Shen, J. Xu, L. Liu, J. Tan, M. Li, N. Xu, S. Luo, J. Wang, F. Yang, J. Tang, Q. Li, Y. Wang, L. Yu, Z. Yan, Liver-targeted siRNA lipid nanoparticles treat hepatic cirrhosis by dual Antifibrotic and anti-inflammatory activities, ACS Nano 14 (2020) 6305–6322.
[70] R. Li, Z. Meng, J. Xie, Effects of sulfur dioxide on the expressions of MUC5AC and ICAM-1 in airway of asthmatic rats, Regul. Toxicol. Pharmacol. 48 (2007) 284–291.

[71] B.-R. Bang, E. Chun, E.-J. Shim, H.-S. Lee, S.-Y. Lee, S.-H. Cho, K.-U. Min, Y.-Y. Kim, H.-W. Park, Alveolar macrophages modulate allergic inflammation in a murine model of asthma, Exp. Mol. Med. 43 (2011) 275–280.
[72] S. Ochiai, F. Jagot, L. Kyle Ryan, E. Hyde, F. White Ruby, M. Prout, J. Schmidt Alfonso, H. Yamane, O. Lamiable, G. Le Gros, F. Ronchese, Thymic stromal lymphopoietin drives the development of IL-13+ Th2 cells, Proc. Natl. Acad. Sci. 115 (2018) 1033–1038.
[73] C.L. Sokol, G.M. Barton, A.G. Farr, R. Medzhitov, A mechanism for the initiation of allergen-induced T helper type 2 responses, Nat. Immunol. 9 (2008) 310–318.
[74] E. Conde, R. Bertrand, B. Balbino, J. Bonnefoy, J. Stackowicz, N. Caillot, F. Colaone, S. Hamdi, R. Houmadi, A. Loste, J.B.J. Kamphuis, F. Huetz, L. Guilleminault, N. Gaudenzio, A. Mougel, D. Hardy, J.N. Snouwaert, B.H. Koller, V. Serra, P. Bruhns, G. Grouard-Vogel, L.L. Reber, Dual vaccination against IL-4 and IL-13 protects against chronic allergic asthma in mice, Nat. Commun. 12 (2021) 2574.
[75] C.M. Evans, K. Kim, M.J. Tuvim, B.F. Dickey, Mucus hypersecretion in asthma: causes and effects, Curr. Opin. Pulm. Med. 15 (2009) 4–11.
[76] A. Nieto-Orellana, H. Li, R. Rosiere, N. Wauthoz, H. Williams, C.J. Monteiro, C. Bosquillon, N. Childerhouse, G. Keegan, D. Coghlan, G. Mantovani, S. Stolnik, Targeted PEG-poly(glutamic acid) complexes for inhalation protein delivery to the lung, J. Control. Release 316 (2019) 250–262.
[77] B.H. Lee, R. Kushwah, J. Wu, P. Ng, N. Palaniyar, S. Grinstein, D.J. Philpott, J. Hu, Adenoviral vectors stimulate innate immune responses in macrophages through cross-talk with epithelial cells, Immunol. Lett. 134 (2010) 93–102.
[78] U. Lappalainen, J.A. Whitsett, S.E. Wert, J.W. Tichelaar, K. Bry, Interleukin-1β causes pulmonary inflammation, emphysema, and airway remodeling in the adult murine lung, Am. J. Respir. Cell Mol. Biol. 32 (2005) 311–318.
[79] S.M. Hurst, T.S. Wilkinson, R.M. McLoughlin, S. Jones, S. Horiuchi, N. Yamamoto, S. Rose-John, G.M. Fuller, N. Topley, S.A. Jones, IL-6 and its soluble receptor orchestrate a temporal switch in the pattern of leukocyte recruitment seen during acute inflammation, Immunity 14 (2001) 705–714.
[80] M. Kendall, P. Ding, R.-M. Mackay, R. Deb, Z. McKenzie, K. Kendall, J. Madsen, H. Clark, Surfactant protein D (SP-D) alters cellular uptake of particles and nanoparticles, Nanotoxicology 7 (2013) 963–973.